LETTER

doi:10.1038/nature22381

Dynamic corticostriatal activity biases social bonding in monogamous female prairie voles

Elizabeth A. Amadei[1,2,3]*, Zachary V. Johnson[1,4,5]*, Yong Jun Kwon[1,3,4], Aaron C. Shpiner[3,6], Varun Saravanan[3,4], Wittney D. Mays[1,3], Steven J. Ryan[1,5], Hasse Walum[1,5], Donald G. Rainnie[1,5], Larry J. Young[1,4,5] & Robert C. Liu[1,3,4]

Adult pair bonding involves dramatic changes in the perception and valuation of another individual[1]. One key change is that partners come to reliably activate the brain's reward system[2–6], although the precise neural mechanisms by which partners become rewarding during sociosexual interactions leading to a bond remain unclear. Here we show, using a prairie vole (*Microtus ochrogaster*) model of social bonding[7], how a functional circuit from the medial prefrontal cortex to nucleus accumbens is dynamically modulated to enhance females' affiliative behaviour towards a partner. Individual variation in the strength of this functional connectivity, particularly after the first mating encounter, predicts how quickly animals begin affiliative huddling with their partner. Rhythmically activating this circuit in a social context without mating biases later preference towards a partner, indicating that this circuit's activity is not just correlated with how quickly animals become affiliative but causally accelerates it. These results provide the first dynamic view of corticostriatal activity during bond formation, revealing how social interactions can recruit brain reward systems to drive changes in affiliative behaviour.

The formation of socially monogamous relationships, or pair bonds, is a complex phenomenon occurring in fewer than 5% of mammalian species[8]. In the monogamous prairie vole, neurochemicals (for example, oxytocin, dopamine)[7] act in two anatomically connected[9,10] corticostriatal areas, the medial prefrontal cortex (mPFC) and nucleus accumbens (NAcc), to establish a selective preference towards a partner[3,4]. Individual variation in neurochemical receptors within this circuit explains differences in affiliative behaviour[4,5]. However, little is known about how mPFC and NAcc are dynamically activated during sociosexual interactions. mPFC–NAcc communication is more generally implicated in an animal's ability to effectively coordinate its behaviour to obtain rewards[11,12], including gaining new behavioural strategies[13]. We therefore hypothesized that mPFC–NAcc functional connectivity helps to switch animals to express affiliative behaviour towards a partner.

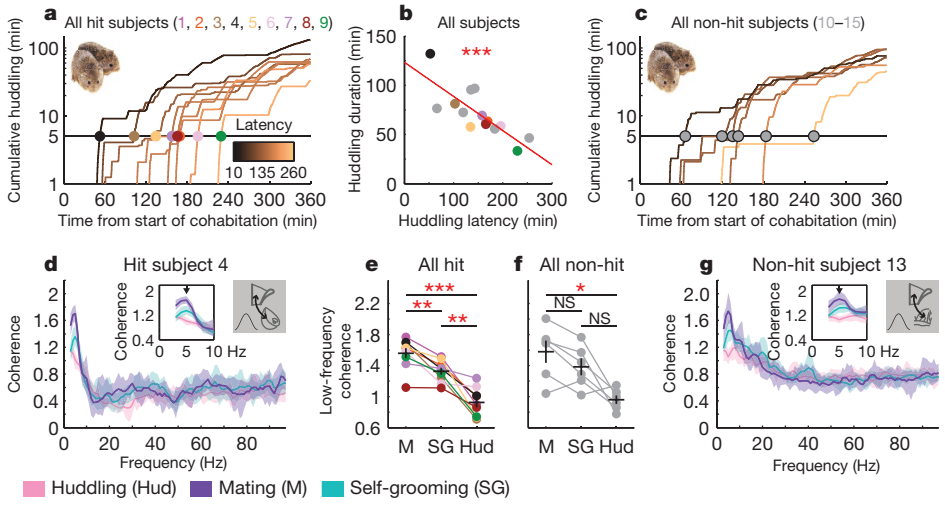

Figure 1 | Mating enhances low-frequency coherence across multiple brain areas. a, **c**, Cumulative huddling trajectories of hit (**a**) and non-hit (**c**) subjects during cohabitation; huddling latencies are indicated by dots colour-coded by subject. **b**, Huddling latency negatively correlates with total huddling duration over full cohabitation ($n = 15$; $R^2 = 0.63$, $P < 0.001$). **d**, **g**, Coherence spectra for example hit (**d**) and non-hit (**g**) subjects, with insets indicating low-frequency peaks during mating (5 Hz). Solid lines and shaded regions show mean and mid-95th percentile range, respectively, of the $n = 40$ coherence estimates for a given behaviour (see Methods). **e**, **f**,The 5 Hz coherence is significantly modulated by behaviour in both hits (**e**; $n = 9$; $F_{2,16} = 35.10$, $P < 0.001$; post hoc, mating (M) versus self-grooming (SG), $t_8 = 4.65$, $P = 0.005$; mating versus huddling (Hud), $t_8 = 6.73$, $P < 0.001$; self-grooming versus huddling, $t_8 = 5.10$, $P = 0.003$) and non-hits (**f**; $n = 6$; $F_{2,10} = 12.43$, $P = 0.002$; post hoc, mating versus self-grooming, $t_5 = 2.44$, $P = 0.176$; mating versus huddling, $t_5 = 4.08$, $P = 0.029$; self-grooming versus huddling, $t_5 = 3.08$, $P = 0.082$). Reported coherence P values are Bonferroni-corrected for multiple comparisons (see Methods). Data are mean ± s.e.m. The rat brain in this Figure, Figs 2 and 3, and Extended Data Figs 2 and 6–10 has been adapted with permission from ref. 14. The image of huddling voles in this Figure, Fig. 3, and Extended Data Figs 6–8 has been adapted with permission from ref. 17.

[1]Silvio O. Conte Center for Oxytocin and Social Cognition, Center for Translational Social Neuroscience, Emory University, Atlanta, Georgia 30322, USA. [2]Wallace H. Coulter Department of Biomedical Engineering, Georgia Institute of Technology and Emory University, Atlanta, Georgia 30332, USA. [3]Department of Biology, Emory University, Atlanta, Georgia 30322, USA. [4]Graduate Program in Neuroscience, Emory University, Atlanta, Georgia 30322, USA. [5]Yerkes National Primate Research Center (YNPRC), Department of Psychiatry and Behavioral Sciences, Emory University, Atlanta, Georgia 30322, USA. [6]Undergraduate Program in Neuroscience and Behavioral Biology, Emory University, Atlanta, Georgia 30322, USA.
*These authors contributed equally to this work.

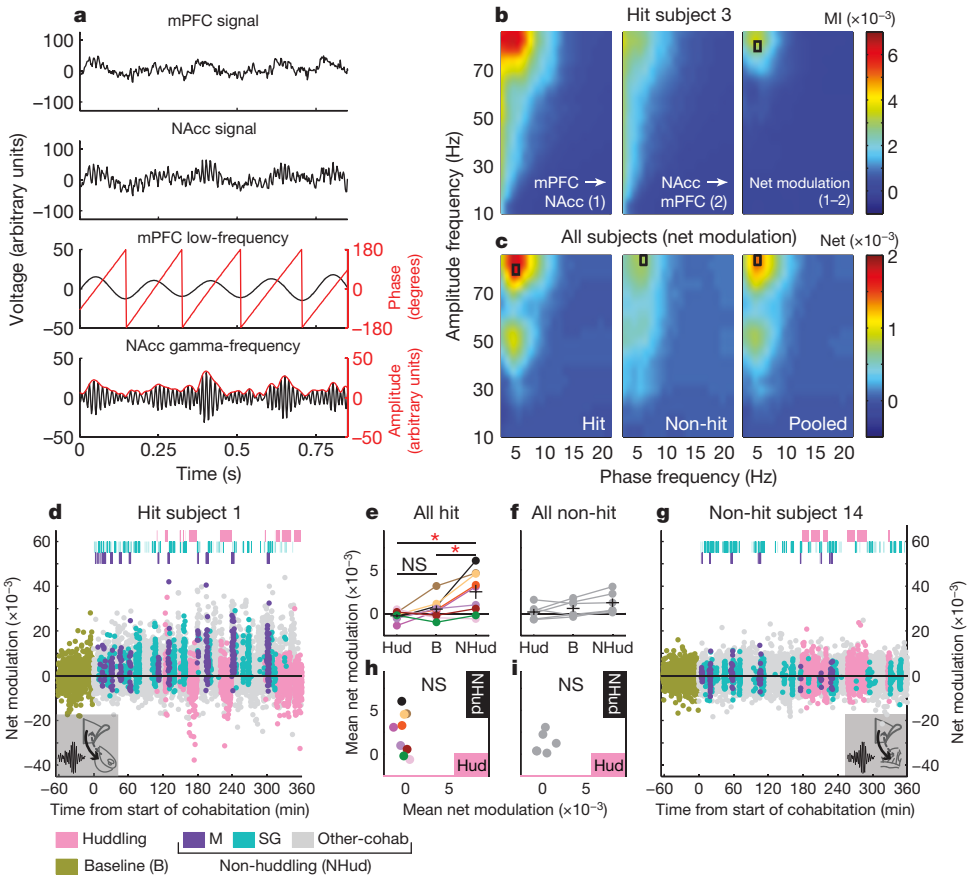

Figure 2 | mPFC–NAcc cross-frequency coupling is dynamically modulated and behaviour-dependent. a, Example raw LFP from mPFC (top) and NAcc (upper middle), filtered into low-frequency (lower middle) and gamma-frequency (bottom) bands, shows gamma amplitude modulation by low-frequency phase. **b**, Modulation index (MI) of phase-amplitude coupling for example hit subject showing mPFC-to-NAcc (left) and NAcc-to-mPFC (middle) directions during cohabitation. Net modulation (right) is the difference in modulation index between directions. **c**, Mean net modulation for hit (left, $n = 9$), non-hit (middle, $n = 6$), or pooled (right, $n = 15$) subjects shows peaks when mPFC low-frequency phase modulates NAcc (or non-hit) gamma amplitude (indicated by black rectangle). **d**, **g**, Net modulation values (2-s, non-overlapping windows) sampled over a baseline solo period (gold points) and 6-h cohabitation for example hit (**d**) and non-hit (**g**) subjects. Values that temporally overlap with mating, self-grooming, and huddling behaviours (top hashes) are colour-coded accordingly. All non-scored values are indicated as 'Other-cohab', which together with mating and self-grooming represent 'non-huddling' values. **e**, **f**, Mean net modulation across subjects during huddling, baseline, and non-huddling (NHud) behaviours in all hits (**e**; $n = 9$) and non-hits (**f**; $n = 6$). Net modulation varies with behaviour in hits ($F_{1.219,9.754} = 9.44$, $P = 0.010$, Greenhouse–Geisser corrected; post hoc, non-huddling versus baseline (B), $t_8 = 3.39$, $P = 0.028$; non-huddling versus huddling, $t_8 = 3.17$, $P = 0.040$; huddling versus baseline, $t_8 = 1.81$, $P = 0.322$) but not non-hits ($F_{1.027,5.133} = 3.94$, $P = 0.102$, Greenhouse–Geisser corrected). **h**, **i**, Non-huddling and huddling net modulations are not correlated in either hits (**h**; $R^2 = 0.10$, $P = 0.417$) or non-hits (**i**; $R^2 = 0.06$, $P = 0.630$). Reported P values in **e**, **f** are Bonferroni-corrected for multiple comparisons (see Methods). Data are mean ± s.e.m.

To examine the neural and behavioural specificity of this hypothesis, we developed an electrophysiological recording approach for freely moving females during sociosexual interactions (Extended Data Fig. 1a–c). Electrodes were chronically implanted (Extended Data Fig. 2) in the mPFC and NAcc (hit animals) or an off-target area posterior to NAcc (within or bordering the bed nucleus of the stria terminalis; non-hit animals), and validated histologically[14]. Synchronized local field potentials (LFPs) and video were acquired during a 6-h cohabitation with a male. Mating, which accelerates bond formation[15], and side-by-side huddling, an index of bond expression[16,17], were assessed as measures of affiliative behaviours during cohabitation. Self-grooming was assessed as a self-directed, high-motion control behaviour.

Behaviours were variable from individual to individual, yet not different overall between hit and non-hit animal groups (Extended Data Fig. 3a). In particular, individuals varied in how quickly they began huddling (huddling 'latency'), with those that started earlier going on to huddle more (Fig. 1a–c). Accelerated huddling latencies were not simply explained by the quantity or timing of mating or self-grooming (Extended Data Fig. 3b), motivating us to ask whether mPFC–NAcc circuit activation could better explain variability in the timing of a switch towards more huddling.

Low-frequency drive from mPFC to NAcc can alter behavioural responses to environmental stimuli[18,19], so we analysed whether mPFC–NAcc connectivity increases during social behaviours that promote more affiliative responses to a partner. Low-frequency coherence, a common measure of functional connectivity, was significantly higher during mating compared with self-grooming and huddling (Fig. 1d, e). Non-hit animals also showed significantly higher low-frequency coherence during mating compared with huddling (Fig. 1f, g), indicating that mating generally enhances low-frequency connectivity across multiple brain areas, consistent with a previous Fos study in males[6].

To assess how this low-frequency connectivity modulates local activity within brain areas, we measured the interaction between low- and high (gamma)-frequency oscillations across brain areas (Fig. 2a). Gamma oscillations reflect local network activation[20], including entrainment of fast-spiking interneurons within the ventral striatum[21–23]. In contrast, lower-frequency rhythms (for example, delta, theta) can regulate gamma oscillations by phase modulating their amplitude[24], a phenomenon observed across brain areas[25]. In both hit and non-hit groups, phase-amplitude coupling ('net modulation', Fig. 2b, c) over the full cohabitation was maximal when low-frequency

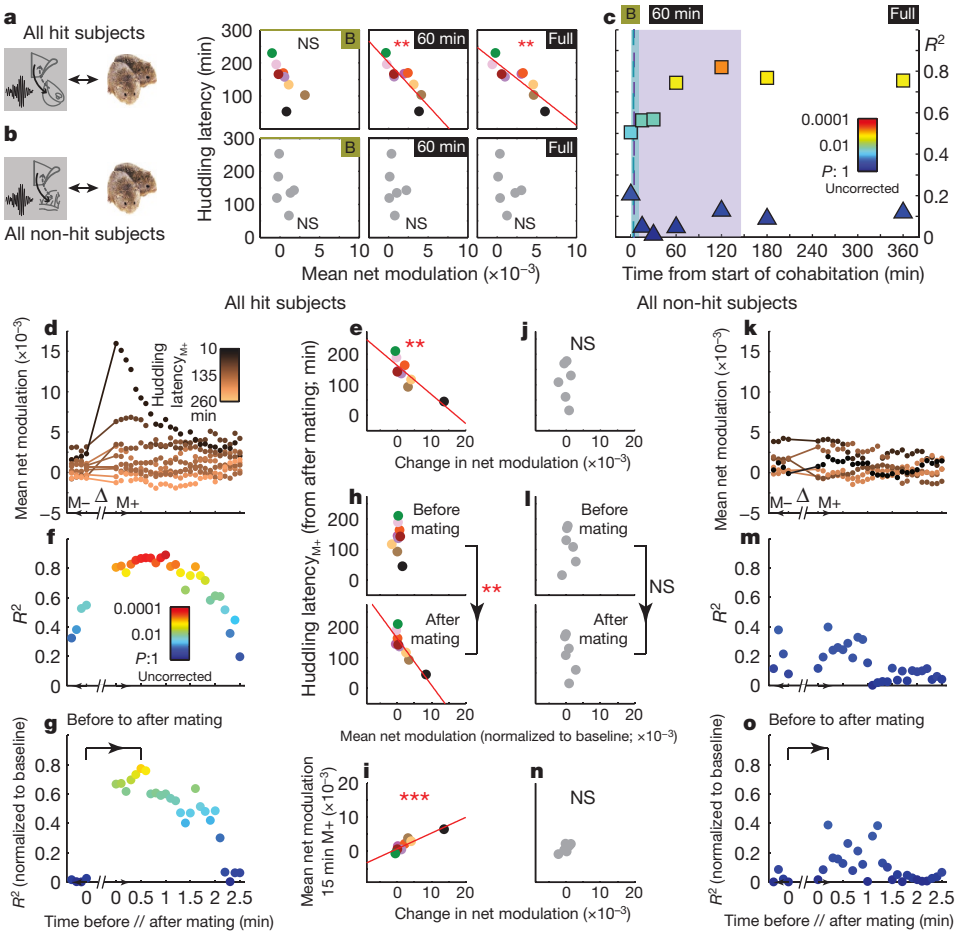

Figure 3 | mPFC–NAcc cross-frequency coupling correlates with huddling latency. **a**, **b**, Correlations between huddling latency and mean non-huddling net modulation during baseline, first 60 min, and full cohabitation in hits (**a**; $n = 9$; $R^2 = 0.51$, $P = 0.096$; $R^2 = 0.74$, $P = 0.008$; $R^2 = 0.76$, $P = 0.007$, respectively) and non-hits (**b**; $n = 6$; $R^2 = 0.21$, $P > 0.99$; $R^2 = 0.05$, $P > 0.99$; $R^2 = 0.12$, $P > 0.99$, respectively). Significant correlations occur for hits at 60 min and full cohabitation. **c**, Correlation strength (R^2) between huddling latency and mean non-huddling net modulation increases for larger time windows from start of cohabitation in hits (squares) but not non-hits (triangles). Shaded regions and dashed bars indicate range and median of latencies to first mating (purple) and self-grooming (green) across all subjects ($n = 15$). **d**, **k**, Mean net modulation values within 1-min moving windows (stepped by 0.1 min) before (M−) and after (M+) the first mating bout of hits (**d**) and non-hits (**k**). Each subject's values are colour-coded by that subject's latency to huddle from the end of the mating bout (latency$_{M+}$). **e**, **j**, Change in mean net modulation from immediately before to after the first mating bout negatively correlates with huddling latency$_{M+}$ in hits (**e**; $R^2 = 0.72$, $P = 0.004$; indicated by line segments in **d**) but not non-hits (**j**; $R^2 = 0.02$, $P = 0.766$; line segments in **k**). **f**, **m**, Strength of correlation between mean net modulation and huddling latency$_{M+}$ increases from before to after mating and is sustained for ~2 min in hits (**f**) but not non-hits (**m**). **g**, **h**, This increase in hits is maintained, and significant ($P = 0.002$, permutation test on difference in R^2 (0.75) between bracketed time-points), when subtracting out the mean baseline net modulation from the local values around mating. **l**, **o**, Non-hits show no significant increase in correlation strength ($P = 0.233$, observed R^2 difference of 0.39). **i**, **n**, Change in mean net modulation from immediately before to after first mating bout correlates with mean non-huddling net modulation in the 15 min after mating in hits (**i**; $R^2 = 0.84$, $P < 0.001$) but not non-hits (**n**; $R^2 = 0.58$, $P = 0.080$). All mating results in hit subjects (**e**, **h**, **i**) remain significant even without subject 4 (black dot, $n = 8$). Reported P values in **a**, **b** are Bonferroni-corrected for multiple comparisons (see Methods).

mPFC activity (5–6 Hz) modulated high gamma (80–84 Hz) activity in either the NAcc or non-hit area, motivating our focus below on this specific oscillatory channel for communication between regions.

Net modulation during the cohabitation period and a pre-cohabitation solo baseline period was dynamically modulated, most prominently in hit animals (Fig. 2d, g and Extended Data Fig. 4). Positive values were consistent with Granger causality estimates showing elevated low-frequency drive from mPFC to NAcc (versus the reverse) during mating (Extended Data Fig. 5). Net modulation varied significantly with behaviours in hit animals only (Fig. 2e, f). Net modulation during huddling was low and comparable to its level during baseline (Fig. 2e), implying that huddling does not elevate functional connectivity between mPFC and NAcc. Low net modulation was not likely from motionlessness, since animals were active and investigative when alone. In contrast, average net modulation during cohabitation outside huddling (non-huddling net modulation), while highly variable across animals, was significantly enhanced compared with both baseline and huddling. In the hit group only, individuals' non-huddling net modulation over the full cohabitation significantly correlated with how quickly they began accumulating huddling (huddling latency, Fig. 3a, b), while huddling net modulation itself was uncorrelated with huddling latency (Extended Data Fig. 6a, b; no correlation between huddling and non-huddling net modulations, Fig. 2h, i). Animals' non-huddling net modulation was not explained by electrode placement (Extended Data Fig. 6c, d), nor by the amount or timing of mating or self-grooming (Extended Data Fig. 6e, f). Therefore, the specific modulation of NAcc activity by the mPFC throughout the full cohabitation, except during huddling, explained how quickly individuals became affiliative.

To determine the temporal emergence of this correlation, we next averaged net modulation over increasing time windows from the start of cohabitation. Baseline net modulation was moderately, albeit

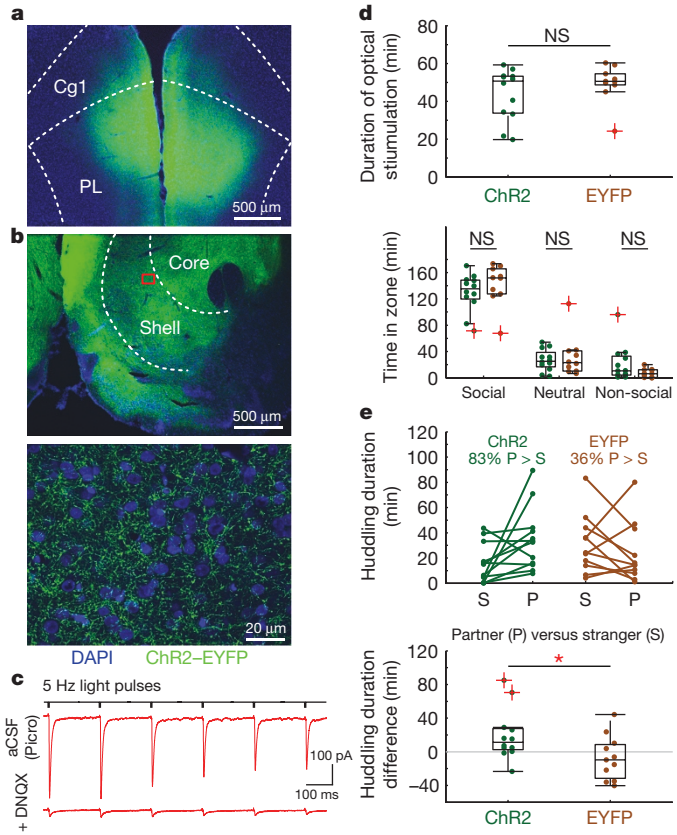

Figure 4 | Low-frequency stimulation of mPFC-to-NAcc projections biases behavioural preference towards a partner. a, **b**, Example immunohistochemistry showing (**a**) ChR2 expression in mPFC (injection site, top image) and (**b**) fibres projecting to NAcc (stimulation site; middle and bottom images; bottom image is magnified view of boxed area). ChR2 tagged with EYFP for visualization. Counterstain with 4′,6-diamidino-2-phenylindole (DAPI) shows cell nuclei. **c**, Light-evoked excitatory postsynaptic currents in example putative NAcc medium spiny neuron during whole-cell patch-clamp recording in presence of picrotoxin (Picro; top). Excitatory transmission confirmed using AMPA/kainate receptor antagonist 6,7-dinitroquinoxaline-2,3-dione (DNQX; bottom). Top and bottom traces each represent average response to $n = 5$ light-pulse trains at 5 Hz (see Methods). **d**, Total optical stimulation (top) and time spent in each zone (bottom) during cohabitation do not significantly differ between ChR2-expressing ($n = 12$) and control subjects (expressing EYFP only, $n = 10$; one subject missing owing to data loss during cohabitation) (stimulation, Cohen's $d = 0.46$, $P = 0.298$; social, $d = 0.41$, $P = 0.345$; neutral, $d = 0.20$, $P = 0.698$; non-social, $d = 0.68$, $P = 0.102$). **e**, Top, time spent with partner (P) versus stranger (S) during PPT for ChR2 ($n = 12$) and EYFP ($n = 11$) subjects. Bottom, ChR2 subjects spent significantly greater relative time with the partner compared with stranger ($d = 0.94$, $P = 0.034$). Boxplots show median and interquartile range. Data points indicated by red cross refer to values whose distance from top or bottom of the box is greater than 1.5 times the interquartile range. Cg1, anterior cingulate cortex (area 1); PL, prelimbic cortex.

non-significantly, correlated with huddling latency in hit animals (Fig. 3a, left), potentially reflecting an individual's affiliative predisposition. No predisposition was found in non-hit animals where the correlation was low and non-significant, both at baseline and across time over cohabitation (Fig. 3b, c), where R^2 values were non-overlapping with those of hit animals. In contrast, in hit animals, non-huddling net modulation became increasingly correlated with huddling latency by 60 min into the cohabitation (Fig. 3a, c), before most animals began huddling, but after experiencing their first mating bout (Extended Data Fig. 3c). Hence, even if a weak affiliative predisposition was reflected in the mPFC–NAcc circuit's baseline activation, early cohabitation experience further strengthened this specific circuit's correlation with huddling.

We next considered which early cohabitation behaviours could drive this strengthening. Mating typically occurred quickly (first bout range demarcated in Fig. 3c and Extended Data Fig. 3c), and its net modulation rose during cohabitation in hit animals, unlike self-grooming, another high net modulation, early behaviour (Extended Data Fig. 7). Given that mating promotes bond formation[15], we tested whether early mating improved the circuit's correlation with huddling. In hit animals only, the change in net modulation from immediately before to after the first mating bout predicted the latency to huddle from the end of the bout. Animals with larger increases in net modulation around first mating, but not first self-grooming, more quickly began accumulating huddling (hits: Fig. 3d, e and Extended Data Fig. 8a, b; non-hits: Fig. 3j, k and Extended Data Fig. 8g, h). The change in the animals' net modulation was not simply explained by behaviours during and around mating (Extended Data Fig. 8m, o), and it specifically correlated with the latency to subsequent huddling (as opposed to subsequent mating or self-grooming, Extended Data Fig. 8n, p).

This mating-triggered change in net modulation augmented the circuit's correlation with huddling latency beyond predisposed levels. The magnitude of the change was not correlated with baseline levels (Extended Data Fig. 8q, r), suggesting a separate effect from any predisposition. Moreover, the correlation between local net modulation values (averaged over 1 min) and huddling latency noticeably increased from the minute just before to up to ~2 min after mating (Fig. 3f). Subtracting out individuals' baseline mean net modulation confirmed a significant augmentation (Fig. 3g, h). No improvement was observed around self-grooming (Extended Data Fig. 8c–e), nor in non-hit animals around either mating or self-grooming (Fig. 3l, m, o and Extended Data Fig. 8i, j, l). In hit animals only, net modulation changes around mating, but not self-grooming, correlated with the subsequent net modulation, averaged up to the shortest huddling latency (that is, 15 min after behaviour) (Fig. 3i, n and Extended Data Fig. 8f, k). Hence, mating specifically altered both the temporally local and more sustained post-mating mPFC-to-NAcc circuit activation in a way that predicted subsequent huddling behaviour: animals whose mPFC modulation of NAcc was more strongly boosted went on to huddle faster, thereby pointing to a new physiological source of individual variability in affiliative behaviour.

To causally test the mPFC–NAcc circuit's sufficiency to accelerate huddling even without mating, we activated the circuit during a restricted cohabitation that prevented mating. This cohabitation does not typically lead to pair bonding, as assessed in the laboratory by a later partner preference test (PPT)[16]. We virally expressed channelrhodopsin-2 (ChR2) or a control fluorophore (enhanced yellow fluorescent protein (EYFP)) in mPFC projection neurons. During the cohabitation, when the female entered a 'social zone' containing a caged male, we optically stimulated (up to 1 h) the mPFC–NAcc pathway at 5 or 6 Hz (Fig. 4a–c and Extended Data Figs 1d, e, 9 and 10), consistent with the frequency of peak mating coherence and net modulation. The ChR2 and EYFP groups showed comparable optical stimulation and time spent in each zone (Fig. 4d), indicating that ChR2 activation did not induce coarse behavioural differences during the restricted cohabitation. However, in the PPT the following day, the ChR2 group showed significantly greater preference for the partner than the stranger (Fig. 4e). Thus, low-frequency oscillatory drive from mPFC to NAcc was sufficient to bias the emergence of affiliative behaviour.

Our data demonstrate a previously unknown mechanism by which a corticostriatal circuit can shift female prairie voles towards increasing social affiliation (huddling). These brain areas play a role in non-social experiments in which animals acquire new behavioural strategies to obtain reward[13,26]. We speculate that the rhythmic action of mPFC on NAcc, which is enhanced by mating, could engage oscillatory-based plasticity mechanisms[27,28] to alter how NAcc responds to partner representations (for example, transmitted from amygdala[29] and hippocampus[30]). Future testing of this hypothesis, and whether the mPFC–NAcc circuit is not only sufficient but also necessary for

increasing affiliative behaviour, will further elucidate this circuit's endogenous contribution to bond formation. Neurochemicals (for example, oxytocin, dopamine[7]) released by sociosexual interactions[10] modulate these brain areas in both females and males[3,4,6], raising the possibility that individual differences in neurochemical receptor densities[4,5] could underlie how strongly this circuit is activated to promote an enduring bond.

Online Content Methods, along with any additional Extended Data display items and Source Data, are available in the online version of the paper; references unique to these sections appear only in the online paper.

Received 16 July 2015; accepted 18 April 2017.
Published online 31 May 2017.

1. Hazan, C. & Shaver, P. Romantic love conceptualized as an attachment process. *J. Pers. Soc. Psychol.* **52,** 511–524 (1987).
2. Bartels, A. & Zeki, S. The neural basis of romantic love. *Neuroreport* **11,** 3829–3834 (2000).
3. Young, L. J., Lim, M. M., Gingrich, B. & Insel, T. R. Cellular mechanisms of social attachment. *Horm. Behav.* **40,** 133–138 (2001).
4. Aragona, B. J. *et al.* Nucleus accumbens dopamine differentially mediates the formation and maintenance of monogamous pair bonds. *Nat. Neurosci.* **9,** 133–139 (2006).
5. Ross, H. E. *et al.* Variation in oxytocin receptor density in the nucleus accumbens has differential effects on affiliative behaviors in monogamous and polygamous voles. *J. Neurosci.* **29,** 1312–1318 (2009).
6. Johnson, Z. V. *et al.* Central oxytocin receptors mediate mating-induced partner preferences and enhance correlated activation across forebrain nuclei in male prairie voles. *Horm. Behav.* **79,** 8–17 (2016).
7. Young, L. J. & Wang, Z. The neurobiology of pair bonding. *Nat. Neurosci.* **7,** 1048–1054 (2004).
8. Kleiman, D. G. Monogamy in mammals. *Q. Rev. Biol.* **52,** 39–69 (1977).
9. Christie, M. J., Summers, R. J., Stephenson, J. A., Cook, C. J. & Beart, P. M. Excitatory amino acid projections to the nucleus accumbens septi in the rat: a retrograde transport study utilizing d[^{3}H]aspartate and [^{3}H]GABA. *Neuroscience* **22,** 425–439 (1987).
10. Ross, H. E. *et al.* Characterization of the oxytocin system regulating affiliative behavior in female prairie voles. *Neuroscience* **162,** 892–903 (2009).
11. Nicola, S. M. The nucleus accumbens as part of a basal ganglia action selection circuit. *Psychopharmacology (Berl.)* **191,** 521–550 (2007).
12. Floresco, S. B. The nucleus accumbens: an interface between cognition, emotion, and action. *Annu. Rev. Psychol.* **66,** 25–52 (2015).
13. Block, A. E., Dhanji, H., Thompson-Tardif, S. F. & Floresco, S. B. Thalamic–prefrontal cortical–ventral striatal circuitry mediates dissociable components of strategy set shifting. *Cereb. Cortex* **17,** 1625–1636 (2007).
14. Paxinos, G. & Watson, C. *The Rat Brain in Stereotaxic Coordinates* compact 6th edn (Academic, 2009).
15. Williams, J. R., Catania, K. C. & Carter, C. S. Development of partner preferences in female prairie voles (*Microtus ochrogaster*): the role of social and sexual experience. *Horm. Behav.* **26,** 339–349 (1992).
16. Ahern, T. H., Modi, M. E., Burkett, J. P. & Young, L. J. Evaluation of two automated metrics for analyzing partner preference tests. *J. Neurosci. Methods* **182,** 180–188 (2009).
17. Lim, M. M. *et al.* Enhanced partner preference in a promiscuous species by manipulating the expression of a single gene. *Nature* **429,** 754–757 (2004).
18. Bagot, R. C. *et al.* Ventral hippocampal afferents to the nucleus accumbens regulate susceptibility to depression. *Nat. Commun.* **6,** 7062 (2015).
19. Britt, J. P. *et al.* Synaptic and behavioral profile of multiple glutamatergic inputs to the nucleus accumbens. *Neuron* **76,** 790–803 (2012).
20. Buzsáki, G. & Wang, X.-J. Mechanisms of gamma oscillations. *Annu. Rev. Neurosci.* **35,** 203–225 (2012).
21. Kalenscher, T., Lansink, C. S., Lankelma, J. V. & Pennartz, C. M. A. Reward-associated gamma oscillations in ventral striatum are regionally differentiated and modulate local firing activity. *J. Neurophysiol.* **103,** 1658–1672 (2010).
22. van der Meer, M. A. & Redish, A. D. Low and high gamma oscillations in rat ventral striatum have distinct relationships to behavior, reward, and spiking activity on a learned spatial decision task. *Front. Integr. Neurosci.* **3,** 9 (2009).
23. Berke, J. D. Fast oscillations in cortical–striatal networks switch frequency following rewarding events and stimulant drugs. *Eur. J. Neurosci.* **30,** 848–859 (2009).
24. Lakatos, P. *et al.* An oscillatory hierarchy controlling neuronal excitability and stimulus processing in the auditory cortex. *J. Neurophysiol.* **94,** 1904–1911 (2005).
25. Tort, A. B. *et al.* Dynamic cross-frequency couplings of local field potential oscillations in rat striatum and hippocampus during performance of a T-maze task. *Proc. Natl Acad. Sci. USA* **105,** 20517–20522 (2008).
26. Ragozzino, M. E., Kim, J., Hassert, D., Minniti, N. & Kiang, C. The contribution of the rat prelimbic-infralimbic areas to different forms of task switching. *Behav. Neurosci.* **117,** 1054–1065 (2003).
27. Jutras, M. J. & Buffalo, E. A. Synchronous neural activity and memory formation. *Curr. Opin. Neurobiol.* **20,** 150–155 (2010).
28. Trimper, J. B., Stefanescu, R. A. & Manns, J. R. Recognition memory and theta–gamma interactions in the hippocampus. *Hippocampus* **24,** 341–353 (2014).
29. Stuber, G. D. *et al.* Excitatory transmission from the amygdala to nucleus accumbens facilitates reward seeking. *Nature* **475,** 377–380 (2011).
30. Okuyama, T., Kitamura, T., Roy, D. S., Itohara, S. & Tonegawa, S. Ventral CA1 neurons store social memory. *Science* **353,** 1536–1541 (2016).

Acknowledgements We thank H.-P. Lipp for Neurologgers; F. Lin for initial testing of Neurologgers; J. Manns, G. Berman, and T. Madsen for methodological feedback and discussions on the manuscript; G. Wong for behavioural scoring; M. Zhang, R. Tangutoori, and R. Stanford for assistance with implant design and construction; the members of the Liu, Young and Rainnie laboratories for training, manuscript feedback, and discussions; L. Matthews and the Yerkes animal care and veterinary staff for vole husbandry and care; G. Feldpausch for custom cage design and machining; and J. LaPrairie and L.-L. Shen for assistance. This work was funded by an Emory Neuroscience Initiative grant (R.C.L., L.J.Y.), National Institute of Mental Health (NIMH) R21MH97187 (R.C.L.), NIMH P50MH100023 (L.J.Y., R.C.L.), National Institute of Neurological Disorders and Stroke R90 DA033462 (V.S.), Emory University Biology Graduate Student Award (E.A.A.), and Office of Research Infrastructure Programs' Primate centers P51OD11132 (YNPRC).

Author Contributions E.A.A. adapted the Neurologger to a vole preparation and designed and performed *in vivo* electrophysiology experiments, which motivated an optogenetics approach; optogenetics experiments were designed and performed by E.A.A. and Z.V.J., assisted by Y.J.K.; Z.V.J. validated viral techniques and performed optogenetics surgeries and histology; S.J.R. and E.A.A. designed slice electrophysiology experiments; Z.V.J. performed all surgeries and histology for slice electrophysiology experiments; S.J.R. performed slice electrophysiology experiments, assisted and supervised by E.A.A. and D.G.R., respectively. E.A.A., Z.V.J., Y.J.K., S.J.R., H.W., A.C.S., V.S., and W.D.M. analysed data; E.A.A. drafted the manuscript; Z.V.J., A.C.S., Y.J.K., S.J.R., H.W., and V.S. contributed to the writing; R.C.L. and L.J.Y. edited the manuscript and supervised all aspects of the study.

Author Information Reprints and permissions information is available at www.nature.com/reprints. The authors declare no competing financial interests. Readers are welcome to comment on the online version of the paper. Publisher's note: Springer Nature remains neutral with regard to jurisdictional claims in published maps and institutional affiliations. Correspondence and requests for materials should be addressed to R.C.L. (robert.liu@emory.edu).

Reviewer Information *Nature* thanks R. Fernald and the other anonymous reviewer(s) for their contribution to the peer review of this work.

METHODS

Animals. All procedures were approved by the Emory University Institutional Animal Care and Use Committee. Experimental subjects (in *in vivo* electrophysiology, *in vivo* optogenetics, slice recording) were adult, sexually naive female prairie voles (*M. ochrogaster*) 76–154 days of age at the start of experiments. Animals were taken from our laboratory-bred colony derived from wild-caught Illinois stock. When possible, they were socially housed in same-sex duos or trios until implant surgeries (if performed), at which time they were separated and housed individually. Food (Laboratory Rabbit Diet HF 5326, LabDiet) and water were given *ad libitum* during a 14:10 h light:dark cycle. Stimulus males used in behavioural experiments were adult, sexually experienced males under 1.5 years of age. Partners and strangers used in PPTs (see below) were matched by age (within 61 days) and weight (within approximately 5 g) for each female. Stimulus females used to prepare strangers were adult, sexually naive, socially housed females under 1 year of age.

Since this is the first study to our knowledge to apply *in vivo* electrophysiology and optogenetic approaches in behaving prairie voles, the target number of experimental subjects was chosen on the basis of published studies in rodents using similar methods[5,19,31].

Surgeries. All surgeries were done under isoflurane anaesthesia. Anterior/posterior coordinates were referenced to the bregma, and dorsal/ventral coordinates were referenced to the top of the skull.

In *in vivo* electrophysiology experiments, females were ovariectomized to homogenize their hormonal state and chronically implanted with electrodes 10–20 days later. Electrodes were individual tungsten microelectrodes (1 MΩ, FHC) stereotaxically targeted to the left mPFC (anterior 2.3–2.4 mm (median 2.35 mm), lateral 0.2–0.5 mm (median 0.3 mm), ventral 2.5–2.7 mm (median 2.6 mm)) and either NAcc (anterior 1.8–2.0 mm (median 1.9 mm), lateral 0.8–0.9 mm (median 0.8 mm), ventral 4.6–4.8 mm (median 4.6 mm)) or bed nucleus of the stria terminalis (anterior 1.05–1.9 mm (median 1.1 mm), lateral 0.8–1.0 mm (median 0.95 mm), ventral 4.45–4.6 mm (median 4.5 mm)), which receives direct mPFC projections in rodents[32,33]. Electrodes were positioned in a fixed implant design (Extended Data Fig. 1a) that interfaced with a connector sitting on top of the skull. The connector in turn interfaced with a Neurologger recording device during experiments (see Experiments). A stainless-steel ground screw (F000CE094, JI Morris) was placed in the right posterior cortex (anterior −2.6 mm, lateral −2.5 mm).

In *in vivo* optogenetics experiments, females underwent virus injection and optical fibre implant surgeries. Animals were bilaterally injected with an adeno-associated virus serotype 5 carrying either ChR2 tagged with EYFP under the control of calmodulin-dependent protein kinase II alpha promoter (AAV5-CaMKIIa-hChR2(H134R)–EYFP–WPRE-PA, 4×10^{12} to 8.5×10^{12} viral molecules per millilitre, UNC Vector Core) or a control fluorophore lacking ChR2 (AAV5-CaMKIIa–EYFP, 4.4×10^{12} to 5.2×10^{12} viral molecules per millilitre, UNC Vector Core) to the mPFC (anterior 2.4 mm, medial ±0.3 mm, ventral 2.7 mm). Injection parameters were 500 nl per side, 5 min injection time and 5 min wait time between the end of injection and retraction of the injector to allow the virus to sufficiently diffuse from the injector needle. Animals were assigned to the ChR2 and control groups by randomly selecting the number of animals in a given cage that would receive ChR2 (either one or two in cages of three; cages of two had one animal in each group by constraint) and counterbalancing across cages to produce as equal number of animals in each group as possible.

Approximately 5 weeks after virus injection, animals were implanted with a bilateral optical cannula (200 μm core diameter, 240 μm outer diameter, 0.22 numerical aperture, 4.5 mm fibre length, 1.5 mm pitch, flat tip, Doric Lenses) targeting the medial NAcc (anterior 1.9 mm, medial ±0.75 mm, ventral 4.5 mm). The light transmission efficiency of the optical cannula was measured before implantation (S140C or S121C, PM100D, ThorLabs). Experiments started 6 weeks (42.0 ± 1.9 days (mean ± s.d.)) after virus injection to allow virus expression in mPFC afferents at the NAcc.

In slice electrophysiology experiments, females underwent the same virus injection surgery as described above, but received only ChR2 virus. Recording experiments in the mPFC and NAcc started 15 and 40–43 days after virus injection, respectively. A longer waiting time was used for NAcc recordings to allow virus expression in mPFC afferents at the NAcc.

Experiments. Before behavioural experiments, all females (experimental subjects, stimulus females) were primed with estradiol benzoate (17-β-estradiol-3-benzoate, Fisher Scientific, daily injections of 1–2 μg dissolved in sesame oil starting 3–4 days before experiments) to induce sociosexual interest in males[34]. The following experiments were performed once on independent experimental subjects.

1. LFP recording in behaving females during cohabitation with a male. LFPs were recorded from the mPFC and NAcc of behaving females using a battery-powered Neurologger[35] chip (1-GB model, New Behaviour). The Neurologger has eight channels (four neural data, two reference, one accelerometer, one infrared synchronization) and samples up to 500 Hz. We chose this over a higher-sampling rate, multichannel, tethered system because of the social nature and long recording duration of our experiments, and the need to minimize the chance that the partner would interfere with recordings.

Before experiments, the Neurologger was programmed with sampling rate and data storage parameters and secured onto the connector on top of the animal's skull (Extended Data Fig. 1a). The device recorded and stored data during the experiment. It was disconnected at the end of the experiment to download data onto a computer for analysis. The sampling rate was 199.805 Hz for all subjects except subject 3 (489.075 Hz). Both sampling rates covered an adequate frequency range for data analysis. Subjects were habituated to the device for at least 1 h on the day before experiments.

On the morning of experiments, the female was briefly anaesthetized under isoflurane to secure the Neurologger and then transferred to a clean cage in the testing room to habituate for at least 10–15 min (up to 1 h). A stimulus male was also brought in to the testing room to habituate. This solo habituation period is referred to as the baseline period. At the end of the baseline, the male was added to the female's cage and the animals were cohabitated for 6 h. Neural and video recording were performed throughout the baseline and cohabitation, and synchronized using periodic timestamps delivered every 100 frames (3.3 s) from a Cleversys Topscan system running on a 32-bit Dell Precision T3500 computer. These timestamps were transmitted as infrared and visible light (LED) pulses that were registered in the Neurologger synchronization channel (samples) and the video recording (frames). The sample and frame indexes of these timestamps were detected and matched using custom-written code in MATLAB (MathWorks). Experiments were performed under a Faraday cage to block 60-Hz electrical noise.

2. Optogenetic stimulation in behaving females during suboptimal cohabitation with a male. A combined video tracking and optical stimulation system was used to stimulate mPFC afferents in the NAcc of socially behaving females (Extended Data Fig. 1d, e). This consisted of a custom-designed, three-chambered Plexiglas arena divided into 'social' (6 × 6 inches), 'neutral' (centre; 6 × 5.5 inches), and 'non-social' (6 × 6 inches) zones. The social and non-social zones contained overturned perforated cups housing a male or remaining empty, respectively. A commutator (1 × 2 FC-FC, 0.22 numerical aperture, Doric Lenses) and video camera (Prosilica GC, Allied Vision Technologies) were positioned over the neutral zone. The commutator interfaced the laser (100 mW, 473 nm, fixed wavelength diode module, Cobolt) and a dual fibreoptic patch cable (200 μm core, 220 μm cladding, 900 μm jacket, Doric Lenses) that plugged into the optical cannula on the female, who had free access to the three zones. The female was tracked using an automated video tracking system (RV2 Video Processor, Tucker Davis Technologies) that detected a red marker positioned directly above her head on the patch cable. Optical stimulation was automatically triggered each time she entered the social zone (RV2 Video Processor and RZ5D Bioamp Processor, Tucker Davis Technologies, see Extended Data Fig. 1d, e) and occurred at a frequency of 5 or 6 Hz with pulse duration of 5 ms for as long as she remained in the social zone. Output from the optical cannula was approximately 30 mW (approximately 15 mW per implanted fibre) on the basis of the output from the patch cable and the transmission efficiency of the optical cannula (measured before implantation). The tracking accuracy for time spent in the social zone (tracked time in social zone compared with human scoring) was at least 86.8% over subjects (tracking data for one subject was excluded due to brief power outage causing data loss during cohabitation, see also Statistics).

On the day of experiments, the female was briefly anaesthetized under isoflurane to connect the patch cable. She was then transferred to the three-chambered arena in the testing room, connected to the commutator, and allowed to habituate for 1 h. At the same time, a non-implanted stimulus female was placed in a second, identical three-chambered arena in the same room and allowed to habituate. Two stimulus males were also brought into the room to habituate. At the end of the habituation, one stimulus male ('partner') was placed and contained in the social zone of the implanted female's cage, and the other male ('stranger') was placed and contained in the social zone of the non-implanted female's cage. This procedure was performed to ensure that the partner and stranger stimulus males received the same experience before partner preference testing.

Animals were cohabitated for a total of 2.5–3 h. Within that period, stimulation was available for 1 h starting from the first entrance of the implanted female into the social zone (laser disconnected at the end of this period). All subjects could therefore receive up to 1 h of light stimulation, although most animals spent some time outside the social zone during this period and thus were not stimulated for the full hour (see Fig. 4d, top). At the end of the cohabitation, the males and non-implanted stimulus female were removed and brought back to the colony. The implanted female was briefly anaesthetized to disconnect the patch cable, placed in a clean cage, and returned to the colony. Because two cohabitation experiments were often run in a given day (typically starting in morning or early afternoon), the ordering of start times was counterbalanced within each experimental group to have similar number of animals starting in the morning and early afternoon.

The following day, the implanted female was tested in a 3-h PPT with her partner from cohabitation and a stranger stimulus male. In this test, which was performed in a different room and cage from the cohabitation, the partner male was tethered with a plastic leash to one side of a three-chambered cage and the stranger male was tethered to the opposite side, as described previously[16]. The female, not connected to any optical cabling, was free to move around the cage and spend time with the partner and stranger. The amount of time the female spent in low-motion social contact (huddling) with the partner and stranger was measured with a Cleversys Topscan automated tracking system (movement criterion of <0.04 (ref. 16) for all subjects) and used to assess the female's preference for the partner (see Statistics). The side of the PPT cage on which the partner was tethered was counterbalanced within each experimental group to control for the partner's location in the testing room. Fresh bedding (Bed-o'Cobs Laboratory Animal Bedding ⅛ inches, The Andersons) was used in each test.

3. Combined electrophysiological recording and optogenetic stimulation in slice preparations of mPFC and NAcc neurons of females. Fifteen to 43 days after ChR2 virus injection, brain slices containing mPFC and/or NAcc were prepared as previously described[36]. In brief, animals were decapitated under isoflurane anaesthesia and brains rapidly removed and immersed in ice-cold cutting solution perfused with 95% oxygen/5% carbon dioxide. Coronal sections (200 μm thick) containing mPFC and/or NAcc were then cut using a VTS-1000 vibrating blade microtome (Leica Microsystems). Slices were kept in oxygenated cutting solution at 32 °C for 1 h before being transferred to a recording chamber with regular artificial cerebrospinal fluid. Slices were imaged using a Leica DM-LFS microscope (Leica Microsystems) captured with SimplePCI software (Hamamatsu) for areas of strong fluorescence within the target region of interest (mPFC or NAcc), and recordings performed as follows.

3a. NAcc. Putative medium spiny neurons were visually identified, patched with a thin-walled borosilicate glass-patch electrode, and held at −70 mV with either DC current injection in current clamp ($n=4$ cells) or voltage clamp ($n=3$ cells) configuration. Recording techniques and equipment were as previously described[36]. Excitatory postsynaptic potentials (or currents) were then evoked with optical stimulation through an optical fibre connected to a solid-state laser (Shanghai Laser & Optics Century) and oriented towards the cell (200 μm core, 488 nm, 0.9–3.4 mW measured at end of fibre). Stimulus trains were either 5 Hz (six pulses at 5 Hz, 1 ms pulse duration, repeated every 4 s for a total of five pulse trains) or individual light pulses (1 ms pulse duration, repeated every 4 s for a total of five pulses) used to compute an average electrophysiological response.

Drugs were applied by gravity perfusion at the required concentration in the circulating artificial cerebrospinal fluid. Drugs used were the $GABA_A$ receptor antagonist picrotoxin (10 μM) and the AMPA/kainate receptor antagonist DNQX (20 μM). All drugs were acquired from Tocris and stored frozen as concentrated stock solutions in distilled water (dH_2O) except DNQX, which was diluted in 50% dimethyl sulfoxide. In recordings in the NAcc, picrotoxin and DNQX were added serially, in that order, with recordings between applications. After experiments, mPFC slices from the same subjects were stored for histological verification of virus expression (see Histology).

3b. mPFC. Recordings in prelimbic mPFC were performed as described above, with the exception that the recorded cells were putative pyramidal neurons and maintained at a membrane potential of −60 mV. Cells were recorded from in the presence of tetrodotoxin (1 μM). Tetrodotoxin was acquired from Tocris and stored frozen as a concentrated stock solution in dH_2O.

Histology. 1. *In vivo* electrophysiology. At the end of experiments, electrode-implanted females were deeply anaesthetized under isoflurane and an electrolytic lesion performed at each electrode site (10 μA for 40–45 s, Midgard Precision Current Source, Stoelting). The animals were then euthanized with carbon dioxide. The brain was removed, stored 1–2 days in 1× phosphate buffered saline (PBS) containing 4% paraformaldehyde at 4 °C, and transferred to 1× PBS containing 30% sucrose at 4 °C until fully fixed. Sections (40 μm thick) were prepared on a freezing sliding microtome (Microm). Sections were stored in cryoprotectant, mounted on slides, and stained with cresyl violet. Slides were coverslipped and then imaged on an Eclipse E800 light microscope (Nikon Instruments). Lesion sites were identified and the section was matched to the most anatomically similar plate in ref. 14. Anatomical landmarks used to match the sections to the plates in ref. 14 included the morphology and position of the corpus callosum and anterior commissure. Subjects with electrodes within or on the medial border of the NAcc were included as hit subjects ($n=9$; see Extended Data Fig. 2a). Subjects with electrodes posterior to the NAcc (within or bordering bed nucleus of the stria terminalis) were included as non-hit subjects ($n=6$; see Extended Data Fig. 2c).

2. *In vivo* optogenetics. Tissue processing: at the end of experiments, subjects were deeply anaesthetized under isoflurane and transcardially perfused with 40 ml 1× PBS followed by 40 ml 4% paraformaldehyde in 1× PBS at a rate of approximately 4 ml min^{-1}. After perfusion, brains were rapidly extracted and post-fixed overnight in 4% paraformaldehyde in 1× PBS and were then transferred to 1× PBS containing 30% sucrose and 0.5% sodium azide. Coronal sections (40 μm thick) were collected using a freezing sliding microtome (Microm) and stored in 1× PBS containing 0.5% sodium azide until immunohistochemical staining.

Immunohistochemistry: all sections from both treatments were subjected to fluorescent immunohistochemical labelling for EYFP. Sections were washed in 1× PBS and blocked with 1× PBS containing 2% normal goat serum (NGS, Fitzgerald) for 1 h before primary incubation with anti-GFP primary antibody (1:1,000, chicken polyclonal, Abcam ab13970) in 1× PBS containing 0.2% Triton-X (1× PBST) and 2% NGS for 48 h at 4 °C. After primary incubation, sections were washed in 1× PBST and incubated in secondary antibody conjugated to a green fluorophore (1:1,000, goat polyclonal anti-chicken, Alexa Fluor 488, ab150169) for 4.5 h in 1× PBST containing 2% NGS. Sections then underwent final washes in 1× PBS before being mounted onto slides. Slides were allowed to dry overnight and then coverslipped with Vectashield Antifade Mounting Medium with DAPI (H-1200, Vector Labs).

Fluorescent microscopy: confocal images were collected using an Orca R2 cooled CCD (charge-coupled device) camera (Hamamatsu Photonics) mounted on a Leica DM 5500B microscope (Leica Microsystems) equipped with a CSU10B Spinning Disk (Yokagawa Electronic) and captured with Simple PCI imaging software (Hamamatsu Photonics). Additional fluorescent images were captured using a QI Imaging Fast 1394 12-bit camera mounted on an Eclipse E800 fluorescent microscope (Nikon Instruments) and captured using MCID Imaging software.

3. Slice electrophysiology. Tissue processing: after electrophysiological recordings in NAcc, 200-μm-thick coronal sections containing the recorded slice as well as sections from the same subject containing mPFC were stored for 1–2 days in 1× PBS containing 4% paraformaldehyde at 4 °C, and transferred to 1× PBS containing 30% sucrose at 4 °C until fully fixed. Immediately before mounting, sections were transferred into and washed in 0.1× PBS and were directly mounted onto slides. Mounted sections were allowed to dry overnight and then coverslipped using Vectashield HardSet Antifade Mounting Medium with DAPI (Vector Labs; H-1500). Dense expression of the ChR2–EYFP transgene in both the mPFC and the NAcc was used as a criterion for inclusion and was confirmed at 60× magnification using an Eclipse E800 fluorescent microscope (Nikon Instruments) for all subjects.

Data analysis. After electrophysiology experiments, subject records ($n=15$ total; nine hit subjects, six non-hit subjects) were added to a custom relational database (Microsoft Excel) used to index animals during analysis. Cohabitation videos were then behaviourally scored and the corresponding neural data extracted and analysed. Subjects were labelled as hits (1–9) or non-hits (10–15). They were ordered by the relative anterior/posterior position of their mPFC recording electrode, with '1' being the most anterior of the hit group, and '10' being the most anterior of the non-hit group.

1. Behavioural scoring. An ethogram was developed to define mating, self-grooming, and huddling behaviours occurring in these experiments (see Extended Data Fig. 1c). These were then scored in experimental videos (Observer XT10) and matched to neural data using linear regression to the most adjacent timestamps (see synchronization procedure described above). For consistency and reliability in scoring, two individuals trained on a test video and scored the experimental videos blindly to each other. The percentage agreement between the two scoring records of a given behaviour, calculated as the percentage of total frames scored consistently for that behaviour (that is, occurring or not), was at least 97.9% for mating, 94.6% for self-grooming, and 92.3% for huddling over all hit subjects, and 99.5% for mating, 95.8% for self-grooming, and 91.1% for huddling over all non-hit subjects. Therefore, we used the intersection of each behaviour's scoring within the two records as the measure of that behaviour. Contiguous segments of intersected scoring are referred to as 'epochs' and used in the following analyses of behavioural scoring.

1a. Trials. Trials were extracted from behaviour epochs that were at least 5 s long and for which the individual scoring records started within 1 s of each other (except for huddling, which used a criterion of starting within 5 s owing to a slower onset of the behaviour). Trials were defined as the first 5 s of the behaviour epochs. Trials were further restricted to be within the 6-h cohabitation. The numbers of 5-s trials of mating for all subjects were (ordered by subject identifier) 46, 72, 22, 15, 55, 26, 12, 89, 21, 47, 23, 48, 21, 21, and 24. The numbers of 5-s trials of self-grooming were 47, 37, 59, 19, 21, 37, 57, 17, 34, 49, 73, 58, 42, 42, and 11. The numbers of 5-s trials of huddling were 45, 24, 24, 37, 26, 48, 41, 13, 4, 51, 27, 57, 44, 14, and 25.

1b. Rasters. For cross-frequency coupling analyses, the cohabitation was broken into 2-s non-overlapping time segments. Time segments fully overlapping within an epoch of mating, self-grooming, or huddling were labelled as that behaviour. All remaining time segments were labelled as 'other-cohab.' Time samples labelled as mating, self-grooming, and 'other-cohab' together made up 'non-huddling' time samples.

1c. Bouts. To capture sequences of a given behaviour, the distances between adjacent behaviour epochs were computed and pooled to create a distribution of distances. A single- or two-term natural exponential function was fitted to this distribution. With a and b as the initial value and decay constant (minus sign) of the first term, respectively, and c and d the initial value and decay constant of the second term, respectively, the fitted values for each behaviour were as follows. The values of a for mating, self-grooming, and huddling were 23,320, 15,222, and 5,347 occurrences, respectively. The values of b were 5.315, 3.089, and 3.481 min, respectively. The values of c were 0, 472.6, and 21.17 occurrences, respectively. The values of d were 0, 0.433, and 0.133 min, respectively. For each behaviour, the decay constant of the largest contributor to the fitted function (5.315, 3.089, 3.481 min for mating, self-grooming, and huddling, respectively) was used as the threshold distance between epochs for inclusion within a given bout.

1d. Latency. Latency was calculated for each behaviour as the delay from a given reference point within the experiment (for example, start of cohabitation) to a later reference point within a behaviour (for example, bout start).

1e. Duration. For each behaviour, epochs within a given time window (for example, full cohabitation, smaller time windows) were pooled to compute the duration of that behaviour.

2. LFP data. LFP data were extracted for trials of each behaviour and inspected for data quality. We had previously observed in early testing of the Neurologger that, owing to its fixed amplification settings, data traces could sometimes hit the upper or lower bounds of the visualization range and become clipped at these. Therefore, as a predetermined criterion for inclusion in LFP analyses using windowed data (that is, trials in Granger causality and coherence analyses; moving windows in cross-frequency coupling analyses, as described below), only those windows whose values were contained within the visualization range were used. Further, subject 7 had a brief, 12.7-s disruption in data recording so this data segment was excluded from LFP analyses. In coherence and Granger causality analyses, the total numbers of 5-s trials excluded for mating (ordered by subject identifier) were 31, 16, 0, 4, 19, 6, 11, 10, 44, 4, 0, 16, 1, 4, and 17 (median of 18.8% of original number of mating trials). The total numbers of 5-s trials excluded for self-grooming were 19, 8, 35, 32, 39, 9, 21, 22, 23, 36, 41, 30, 70, 28, and 67 (median of 40.0% of original number of self-grooming trials). The total numbers of 5-s trials excluded for huddling were 2, 1, 4, 4, 6, 2, 0, 0, 2, 0, 5, 0, 0, 0, and 2 (median of 4.0% of original number of huddling trials). In cross-frequency coupling analyses, the percentages of 2-s windows excluded were 10.9, 9.9, 11.5, 24.4, 28.0, 15.4, 11.6, 15.5, 23.5, 20.1, 13.8, 9.0, 15.8, 12.0, and 27.7% (median of 15.4% of original number of windows). The original number of windows ranged from 11,176 to 12,642 (median 12,613).

Coherence, Granger causality, and cross-frequency coupling were computed between brain regions. All analyses were done in MATLAB unless otherwise noted.

2a. Coherence. Coherence analyses were performed using multitaper methods[37] implemented in Chronux (http://chronux.org)[38]. This consisted of multiplying each data segment by a set of orthogonal Slepian tapers[39] specifying a spectral concentration bandwidth $\pm W$. W and the segment duration (T) constrain the maximum number of effectively concentrating tapers to be less than or equal to $2TW - 1$. Parameters used here were $W = 2$ Hz, $T = 1$ s, and three tapers. Coherence was then calculated as the magnitude of the coherency[40]. Coherence ranged from 0 to 1, where a value of 1 represented a perfectly consistent phase and amplitude relationship across tapers and trials.

Coherence estimates were sampled at 1-Hz resolution from 3 Hz to 242 Hz (subject 3) or 3 Hz to 97 Hz (remaining subjects). This range represented the nearest integer above W that was consistent across subjects to the nearest integer below the (Nyquist frequency $- W$).

Inter-behaviour comparisons: coherence was compared between 5-s trials of mating, self-grooming, and huddling (number of trials listed in Data Analysis, paragraph 1a). To address the possibility of non-stationarity in the data, each trial was split into 40, 1-s segments stepped by 0.1 s. Coherence was calculated across trials for each time segment, giving 40 estimates for a given behaviour. These estimates were transformed and bias-corrected, as described in Statistics. They were then averaged to give full-trial estimates of a given behaviour. Statistical testing was performed on these averages. In addition, the 2.5–97.5th percentile range of the 40 estimates was extracted as a measure of variability (prctile function in MATLAB).

2b. Cross-frequency coupling. Cross-frequency coupling was computed using the modulation index[41] metric (code courtesy of A. Tort and T. Madsen). The modulation index quantifies the extent to which the low-frequency phase of one signal modulates the higher-frequency amplitude of another. In brief, the two signals are filtered in low- and high-frequency bands, then Hilbert transformed to obtain the phase and amplitude envelope, respectively. This gives matched phase and amplitude values that are then binned into 20° phase bins. Amplitudes are averaged within each phase bin, giving a distribution of amplitudes over phase bins. This distribution is normalized to the sum of averaged amplitudes. The modulation index is computed as the normalized Kullback–Leibler distance of this distribution from a uniform (flat/unmodulated) distribution.

The modulation index was computed over the course of the experiment for each subject ('MI raster'). The baseline and cohabitation periods were broken into 5-s or 2-s non-overlapping time segments. Five-second segments were used to analyse the spectrum of the modulation index, and 2-s segments were used to relate the modulation index to behaviour (see below). The modulation index was computed on each segment in two directions: (1) mPFC low-frequency phase modulating NAcc (or off-target) gamma amplitude; and (2) NAcc (or off-target) low-frequency phase modulating mPFC gamma amplitude. This consisted of switching which signals were low- or high-frequency filtered (filtering done using the EEGLAB[42] package for MATLAB, eegfilt function).

Five-second time segments (modulation index spectrum): modulation index was computed at multiple combinations of phase and amplitude frequencies. Phase frequencies ranged from 3 to 21 Hz, with integer spacing and bandwidth ± 0.5 Hz. Amplitude frequencies ranged from 32 to 84 Hz, with spacing of 4 Hz and bandwidth ± 2 Hz. To measure the relative strength of the modulation index in the mPFC-to-NAcc direction ('net modulation') at a given phase/amplitude frequency combination, the modulation index computed for the NAcc-to-mPFC direction was subtracted from that of the mPFC-to-NAcc direction. The net modulation was averaged across all time segments and hit animals to identify the frequency combination producing maximal net modulation. The same analysis was performed on non-hit animals.

Two-second time segments (modulation index and behaviour): net modulation was computed at a phase frequency of 5 Hz and amplitude frequency of 80 Hz. These time segments were matched to raster time samples coded as specific behaviours (see Data analysis, paragraph 1b) and averaged across values coded as the same behaviour to estimate the net modulation during that behaviour. Averages were taken over the full cohabitation as well as shorter time segments (for example, within first or last mating bout).

2c. Granger causality. Granger causality was computed with parametric methods[43,44] implemented in code by S. de Waele and N. J. Killian and adapted for use by V.S. and E.A.A. Granger causality tests the degree to which previous values of one time series improve the prediction of a different time series[45] and was used here to assess the directional influence of one brain area over another's activity[46] during mating. Granger causality can be formulated in the frequency domain by fitting and frequency-transforming a bivariate autoregressive model to the two time series[43] (here, mPFC and NAcc LFPs during mating). The power of each time series can then be estimated and decomposed into an intrinsic component and a causal component contributed by the other time series. Granger causality is computed as the natural log of the ratio of the total power (intrinsic + causal) to the intrinsic power.

To fit the autoregressive model, the average values of the time series were subtracted out to produce means of 0 and model parameters estimated using the Nuttall–Strand method. The model order was selected using the combined information criterion[47].

Granger causality was compared in the mPFC-to-NAcc and NAcc-to-mPFC directions during mating (see Statistics). As in the coherence estimates, 5-s trials of mating were split into 40, 1-s segments shifted by 0.1 s. Granger causality was computed on each segment (see below) at integer frequencies from 0 Hz to 244 Hz (subject 3) or to 99 Hz (all other subjects), and then averaged over segments to get a full-trial estimate. The 2.5–97.5th percentile range of the 40 estimates was extracted as a measure of variability. The upper bound of the frequency range represented the nearest integer below the Nyquist frequency.

Granger causality was calculated using a bootstrapping procedure. In brief, for a subject with n trials of mating, n segments matched in time were extracted from the trials. One thousand artificial sets of n segments were generated by randomly selecting with replacement from possible segments. Autoregressive model parameters were averaged across segments in each set, and these average values used to compute Granger causality in the two directions. The actual Granger causality values were defined as the mean over all sets.

Statistics. No statistical methods were used to predetermine sample size.

Statistical tests used a significance level $\alpha = 0.05$ ($^*P < 0.05$, $^{**}P < 0.01$, $^{***}P < 0.001$). Statistical analyses were performed separately on hit ($n = 9$) and non-hit ($n = 6$) groups.

Correlation analyses used the Pearson correlation (corr in MATLAB) and reported R^2 and P values. Linear regression was performed using the polyfit function in MATLAB.

In tests of paired samples, a two-sided Lilliefors test (lillietest in MATLAB) was used to test the normality of the difference between samples. This test was also used to test the normality of individual groups for analyses of variance (ANOVAs). Since this test was less sensitive to small sample sizes, data were also visually inspected

for any obvious skew. Parametric (two-tailed *t*- and ANOVA) tests were used when justified by these analyses.

The Bonferroni method was used to correct for multiple comparisons. The number of corrections and other figure-specific statistical methods are described below. *P* values are not corrected unless otherwise specified.

Fig. 1. To compare mPFC–NAcc coherence between mating, self-grooming, and huddling, the 40 within-trial coherence estimates for each of these behaviours were first Fisher-transformed. They were then bias-corrected for different sample sizes (here: number of trials of each behaviour), as described[48]. Upon averaging these 40 estimates to get a full-trial estimate, the peak frequency of mating coherence was determined for each subject (ranging from 4 to 6 Hz), and the mode of these frequencies across subjects (5 Hz) was used for inter-subject comparisons. The effect of behaviour on coherence was tested using a one-way repeated-measures ANOVA with behaviour as the within-subject factor (SPSS). Sphericity was verified using Mauchly's test (SPSS, $W = 0.60$, $P = 0.167$). The difference in coherence between (1) mating and self-grooming, (2) mating and huddling and (3) self-grooming and huddling at 5 Hz was tested for significance using a post hoc two-tailed paired *t*-test (ttest in MATLAB), with correction for three comparisons.

The same analysis was performed on non-hit animals, with coherence evaluated at 5 Hz. Sphericity was verified using Mauchly's test ($W = 0.62$, $P = 0.380$).

Fig. 2. The effect of behaviour (huddling, baseline, non-huddling) on mPFC–NAcc net modulation was tested using a one-way repeated-measures ANOVA with behaviour as the within-subject factor (SPSS). Sphericity was violated (Mauchly's test; $W = 0.36$, $P = 0.028$) and so the Greenhouse–Geisser correction was applied. The difference in net modulation between (1) non-huddling and huddling, (2) non-huddling and baseline, and (3) huddling and baseline was tested for significance using a post hoc two-tailed paired *t*-test (ttest in MATLAB), with correction for three comparisons. The same ANOVA was performed on non-hit animals, with Greenhouse–Geisser correction applied owing to violation of sphericity (Mauchly's test; $W = 0.05$, $P = 0.003$).

Fig. 3. Correlations between huddling latency and non-huddling net modulation during the baseline period, first 60 min of cohabitation, and full cohabitation were corrected for three comparisons.

A permutation test was used to test whether the correlation between huddling latency and non-huddling net modulation significantly improved from before to after mating. The before time-point was that immediately before mating. The after time-point was that producing the highest correlation between net modulation and huddling latency within 3.5 min after mating (see Fig. 3g, o; bracket indicates before and after points). In brief, at both before and after time-points, net modulation values were randomized across subjects (using datasample in MATLAB; same randomized identifiers used in before and after time-points) and then correlated with the huddling latency (kept in subject order). The difference in R^2 (absolute value) between these two correlations was then computed. This re-sampling procedure was repeated 1×10^6 times to produce a permuted (null) distribution of R^2 differences. A two-sided *P* value was obtained as the proportion of shuffled R^2 differences that were greater than the observed value.

Fig. 4. In optogenetics analyses, the relative time spent with the partner in the PPT (partner time minus stranger time) was compared between treatment (expressing ChR2) and control (expressing control fluorophore lacking ChR2) groups using a permutation test. This test was chosen owing to normality violations in group and residual values (discouraging an ANOVA approach). The permutation test involved calculating the effect size (Cohen's d[49] (absolute value)) of the difference between treatment and control groups in the relative time spent with the partner. This observed Cohen's *d* was then compared with a permuted distribution of Cohen's *d* values created by randomly assigning data values without replacement to treatment and control groups (using randperm in MATLAB). The re-sampling procedure was performed 1×10^6 times. A two-sided *P* value was obtained as the proportion of shuffled Cohen's *d* values that were greater than the observed value.

The same permutation approach was used to compare the total duration of optical stimulation as well as time spent in the social, neutral, and non-social zones (see Extended Data Fig. 1d) during cohabitation between treatment and control groups. Owing to a brief power outage after the optical stimulation period for one control animal, video and tracking data for that subject were lost even though it received normal stimulation. Therefore, the number of control subjects used in the optical stimulation and zone analyses is one less than that used in the PPT analyses described above ($n = 10$ as opposed to 11).

Extended Data Fig. 3. The number of bouts, duration and latency of mating, self-grooming, and huddling were compared between hit and non-hit groups using Wilcoxon signed-rank tests (signrank in MATLAB). *P* values were corrected for nine comparisons.

Correlations between huddling latency and mating and self-grooming duration and latency parameters were corrected for eight comparisons.

The effect of behaviour on latency was assessed with a Friedman test because of violations of normality. The difference in latency between (1) mating and self-grooming, (2) mating and huddling, and (3) self-grooming and huddling was tested for significance using a post hoc Wilcoxon signed-rank test, with correction for three comparisons.

Extended Data Fig. 5. To compare Granger causality in the mPFC-to-NAcc and NAcc-to-mPFC directions, Granger causality values in each direction were obtained for each subject at 5 Hz, the same frequency used in coherence comparisons. The difference of the two directions (mPFC-to-NAcc minus NAcc-to-mPFC) across subjects was tested for significance using a two-tailed paired *t*-test.

Extended Data Fig. 7. To calculate the mean net modulation during early and late mating for each subject, net modulation values coded as mating were taken from that subject's first and last mating bouts, respectively, and then averaged. The numbers of values within the first bout were (in subject order) 19, 41, 38, 25, 62, 24, 22, 101, 84, 36, 20, 22, 10, 21, and 31. The numbers of values within the last bout were (in subject order) 48, 52, 24, 26, 70, 34, 35, 57, 38, 45, 33, 33, 20, 24, and 25. To calculate the mean net modulation during early and late self-grooming for each subject, net modulation values coded as self-grooming were taken from that subject's start (moving forward) or end (moving backward) of the cohabitation. The number of self-grooming values were matched to that subject's first and last mating bout (listed above), respectively. The difference of early and late mean net modulation for each behaviour across subjects was performed using a Wilcoxon signed-rank test and Bonferroni-corrected for two comparisons.

Extended Data Fig. 8. The same permutation test described for Fig. 3 was used to test whether the correlation between huddling latency and non-huddling net modulation significantly improved from before to after self-grooming (Extended Data Fig. 8e, i).

Code availability. MATLAB code written to analyse LFP data in this study is available from the corresponding author upon reasonable request.

Data availability. The data that support the findings of this study are available from the corresponding author upon reasonable request. Source Data for all figures with graphical representations are provided in the online version of the paper.

31. Gruber, A. J., Hussain, R. J. & O'Donnell, P. The nucleus accumbens: a switchboard for goal-directed behaviors. *PLoS ONE* **4,** e5062 (2009).
32. Vertes, R. P. Differential projections of the infralimbic and prelimbic cortex in the rat. *Synapse* **51,** 32–58 (2004).
33. Gutman, D. A. *et al.* A DTI tractography analysis of infralimbic and prelimbic connectivity in the mouse using high-throughput MRI. *Neuroimage* **63,** 800–811 (2012).
34. Donaldson, Z. R., Spiegel, L. & Young, L. J. Central vasopressin V1a receptor activation is independently necessary for both partner preference formation and expression in socially monogamous male prairie voles. *Behav. Neurosci.* **124,** 159–163 (2010).
35. Etholm, L., Arabadzisz, D., Lipp, H. P. & Heggelund, P. Seizure logging: a new approach to synchronized cable-free EEG and video recordings of seizure activity in mice. *J. Neurosci. Methods* **192,** 254–260 (2010).
36. Ryan, S. J. *et al.* Spike-timing precision and neuronal synchrony are enhanced by an interaction between synaptic inhibition and membrane oscillations in the amygdala. *PLoS ONE* **7,** e35320 (2012).
37. Mitra, P. P. & Pesaran, B. Analysis of dynamic brain imaging data. *Biophys. J.* **76,** 691–708 (1999).
38. Mitra, P. & Bokil, H. *Observed Brain Dynamics* (Oxford Univ. Press, 2008).
39. Slepian, D. & Pollack, H. O. Prolate spheroidal wave functions, Fourier analysis and uncertainty – I. *Bell Syst. Tech. J.* **40,** 43–63 (1961).
40. Jutras, M. J., Fries, P. & Buffalo, E. A. Gamma-band synchronization in the macaque hippocampus and memory formation. *J. Neurosci.* **29,** 12521–12531 (2009).
41. Tort, A. B., Komorowski, R., Eichenbaum, H. & Kopell, N. Measuring phase-amplitude coupling between neuronal oscillations of different frequencies. *J. Neurophysiol.* **104,** 1195–1210 (2010).
42. Delorme, A. & Makeig, S. EEGLAB: an open source toolbox for analysis of single-trial EEG dynamics including independent component analysis. *J. Neurosci. Methods* **134,** 9–21 (2004).
43. Brovelli, A. *et al.* Beta oscillations in a large-scale sensorimotor cortical network: directional influences revealed by Granger causality. *Proc. Natl Acad. Sci. USA* **101,** 9849–9854 (2004).
44. Dhamala, M. in *Encyclopedia of Computational Neuroscience* (eds. Jaeger, D. & Jung, R.) 2789–2793 (Springer, 2014).
45. Granger, C. W. J. Investigating causal relations by econometric models and cross-spectral methods. *Econometrica* **37,** 424–438 (1969).
46. Gregoriou, G. G., Gotts, S. J., Zhou, H. & Desimone, R. High-frequency, long-range coupling between prefrontal and visual cortex during attention. *Science* **324,** 1207–1210 (2009).
47. de Waele, S. & Broersen, M. T. Order selection for vector autoregressive models. *IEEE Trans. Signal Process.* **51,** 427–433 (2003).
48. Bokil, H., Purpura, K., Schoffelen, J.-M., Thomson, D. & Mitra, P. Comparing spectra and coherences for groups of unequal size. *J. Neurosci. Methods* **159,** 337–345 (2007).
49. Cohen, J. A power primer. *Psychol. Bull.* **112,** 155–159 (1992).

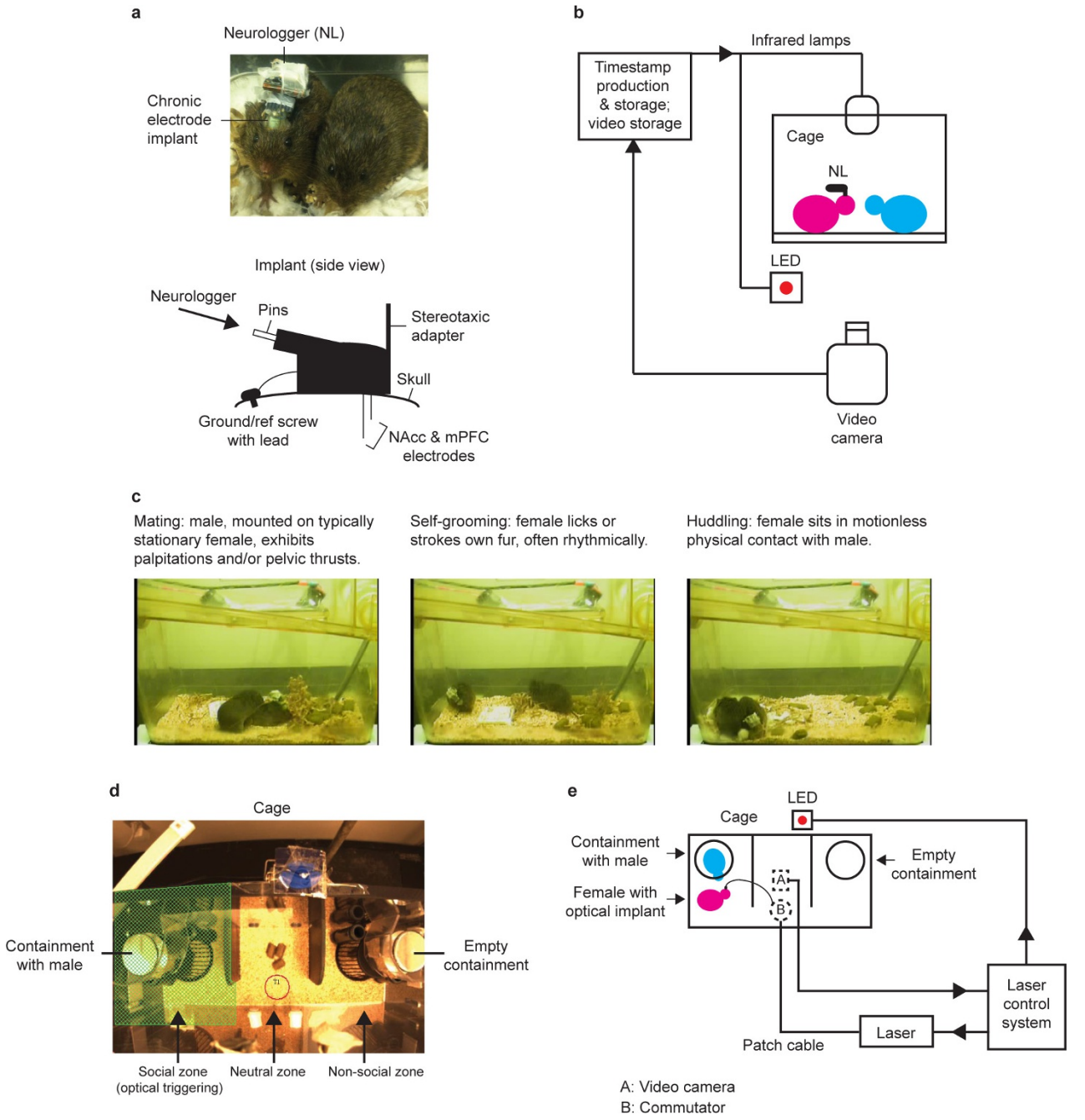

Extended Data Figure 1 | Preparations for electrophysiological and optogenetic experiments. a, Neurologger recording device secured to a female during cohabitation with a male. Neurologger interfaces with a chronic electrode implant targeting mPFC and NAcc. **b**, Schematic of experimental setup. Simultaneous video and neural recording is synchronized by periodic timestamps. **c**, Summarized ethogram definitions of mating, self-grooming, and huddling used to score experimental videos. **d**, Arena used for cohabitation in optogenetics experiments. Arena is divided into social, neutral, and non-social zones. Food is placed in the centre of the neutral zone. Male is contained under a cup in the social zone, and female, implanted with optical fibres, is allowed to freely explore the arena. Optical stimulation is triggered whenever she is in the social zone (green hatched area; red circle is visualization of tracking) for up to 1 h within the cohabitation period. Social zone is defined as consistently as possible across experiments on the basis of physical features of arena. **e**, Schematic of cohabitation setup, additionally showing how laser is controlled by video recording to automatically deliver optical stimulation when female is in the social zone.

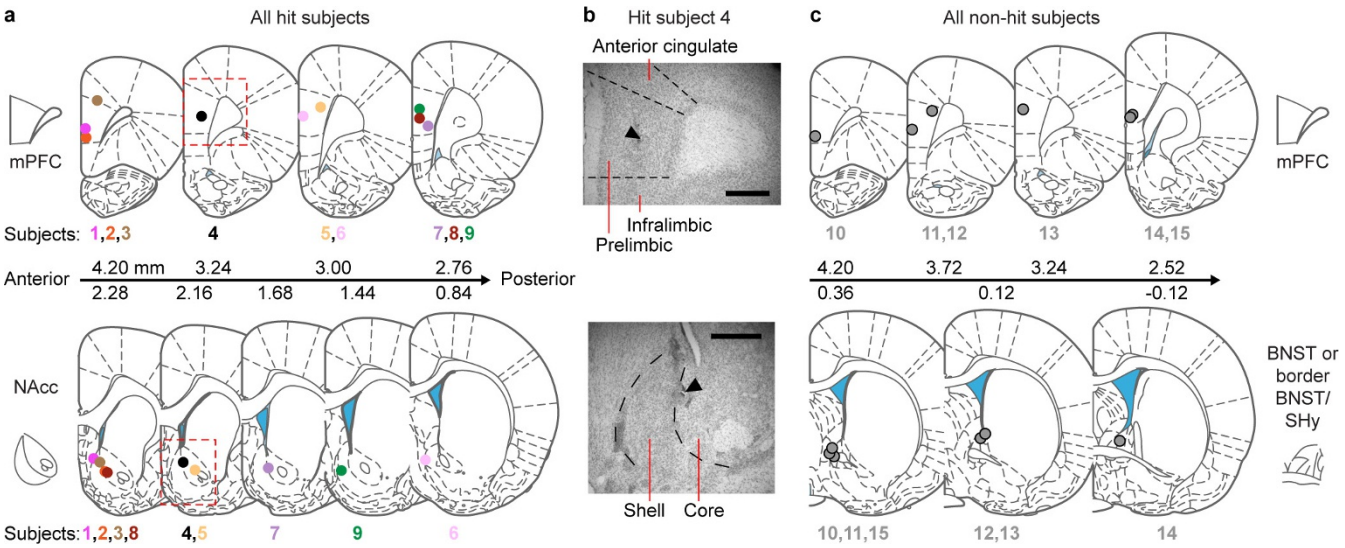

Extended Data Figure 2 | Placement of LFP electrodes in all subjects. **a**, **b**, Electrodes in hit subjects ($n = 9$) targeting mPFC and NAcc (**a**), verified with electrolytic lesions (**b**; scale bar, 500 μm). Anterior/posterior locations of brain sections (units of rat brain atlas[14]; see Methods) are indicated. **c**, Electrodes in non-hit subjects ($n = 6$) targeting mPFC and posterior to NAcc (within or bordering the bed nucleus of the stria terminalis (BNST)). SHy, septohypothalamic nucleus.

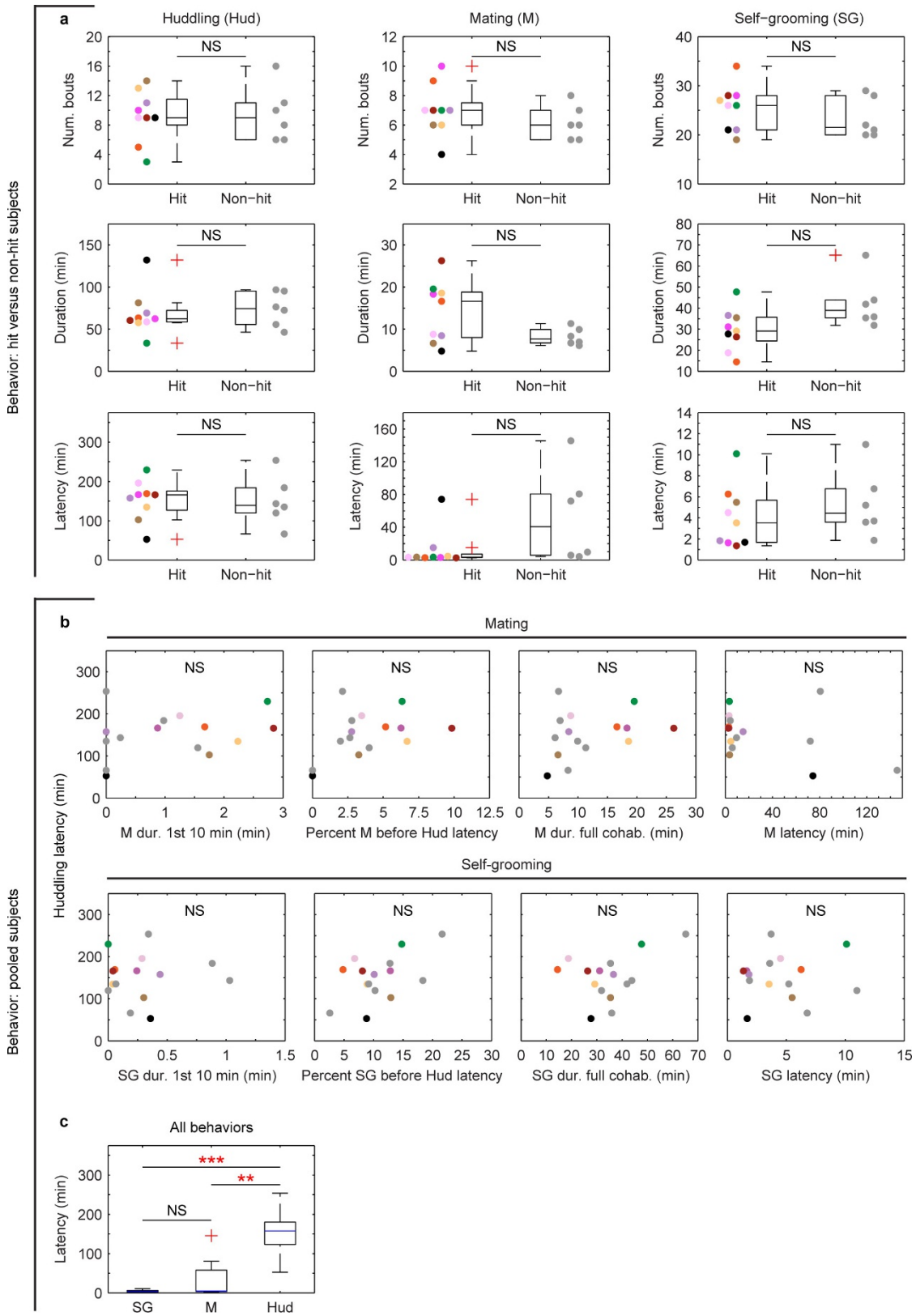

Extended Data Figure 3 | Behavioural characterization of hit and non-hit subjects. a, Number of bouts, total duration, and latency for mating, self-grooming, and huddling in hit ($n = 9$) and non-hit ($n = 6$) subjects. No significant differences exist between subject groups (all $P > 0.05$). **b**, Measures of mating and self-grooming duration and latency do not correlate with huddling latency ($n = 15$; all $P > 0.05$). 'Percent M [or SG] before Hud latency' refers to percentage of time each animal spent mating or self-grooming before reaching its huddling latency. **c**, Latency is modulated across behaviours ($n = 15$; $\chi^2_2 = 18.53$, $P < 0.001$, Friedman test), with mating and self-grooming showing shorter latencies compared with huddling but similar latencies to each other (self-grooming versus huddling, $P < 0.001$; mating versus huddling, $P = 0.001$; mating versus self-grooming, $P = 0.454$, Wilcoxon signed-rank test). Reported P values in **a**–**c** are Bonferroni-corrected for multiple comparisons (see Methods). Boxplots show median and interquartile range.

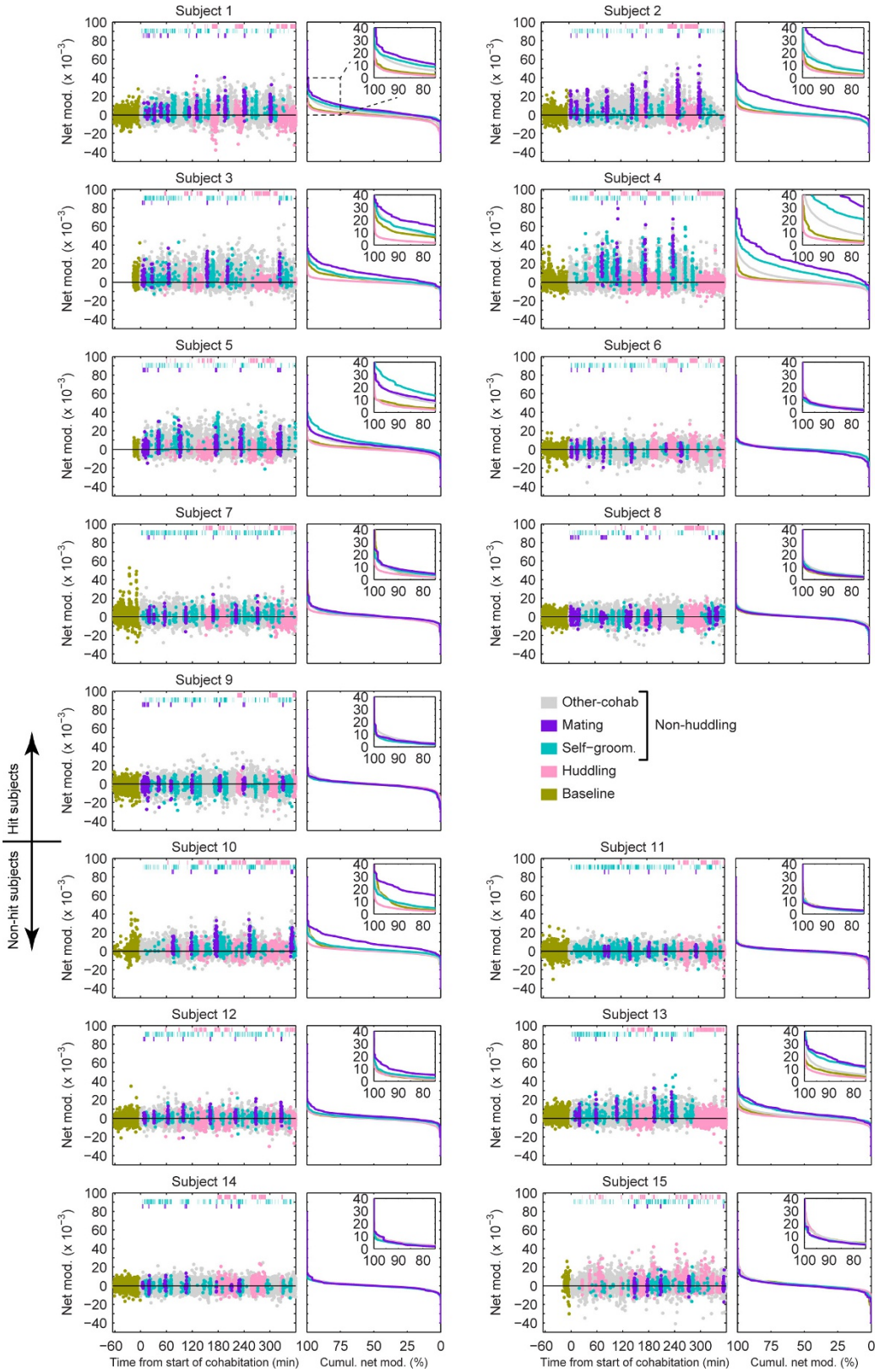

Extended Data Figure 4 | Net modulation data for all subjects. Net modulation values (2-s, non-overlapping windows) sampled over a baseline solo period (gold points) and 6-h cohabitation for all hit (numbers 1–9) and non-hit (numbers 10–15) subjects. Values that temporally overlap with mating, self-grooming, and huddling behaviours (top hashes) are colour-coded accordingly. All non-scored values are indicated as 'other-cohab,' which together with mating and self-grooming represent 'non-huddling' values. Cumulative distributions of net modulation values coded by behaviour are shown in the right panel for each subject.

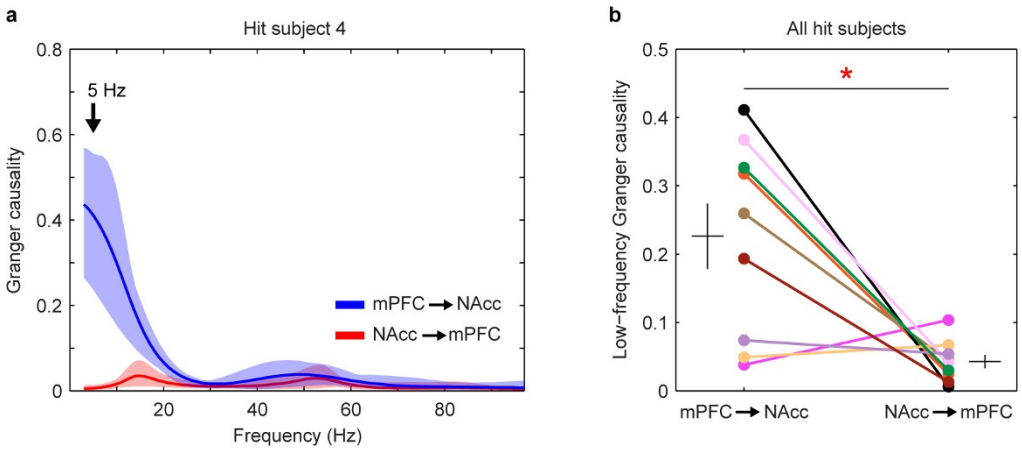

Extended Data Figure 5 | Granger causality in mPFC–NAcc circuit during mating. a, Granger causality spectra in the mPFC-to-NAcc and NAcc-to-mPFC directions for example subject. Solid lines and shaded regions show mean and mid-95th percentile range, respectively, of the $n = 40$ Granger causality estimates for a given brain-area direction (see Methods). **b**, Comparison of Granger causality at 5 Hz in the two directions across hit subjects ($n = 9$). Granger causality is significantly higher in the mPFC-to-NAcc direction ($t_8 = 3.29$, $P = 0.011$). Data are mean ± s.e.m.

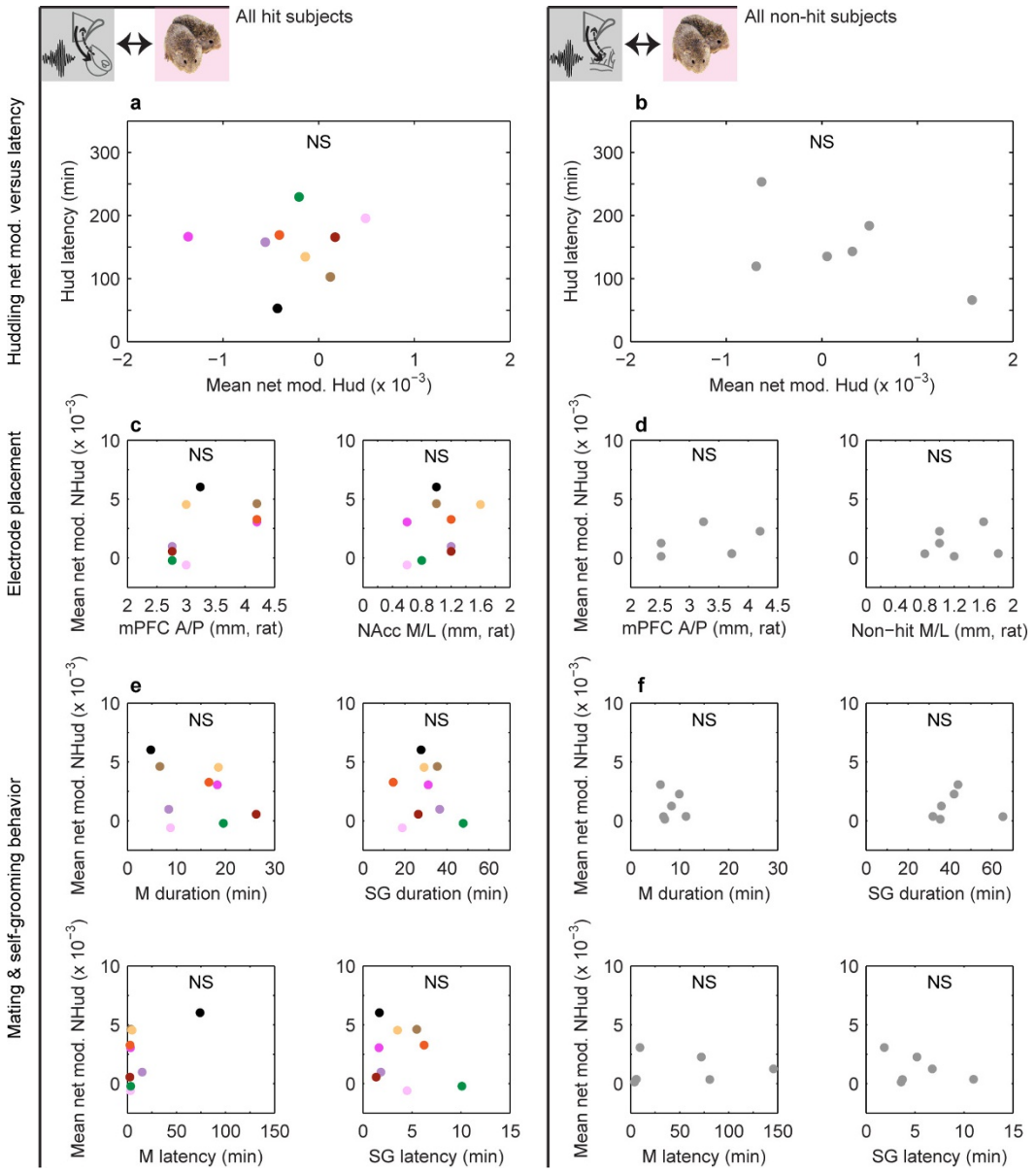

Extended Data Figure 6 | Specificity of correlation between non-huddling net modulation and huddling latency. a, **b**, Mean huddling net modulation is uncorrelated with huddling latency in hits (**a**; $n = 9$) and non-hits (**b**; $n = 6$) (all $P > 0.05$). **c**, **d**, Mean non-huddling net modulation is uncorrelated with electrode placement (mPFC anterior (A)–posterior (P) location or NAcc/non-hit medial (M)–lateral (L) location; units of rat brain atlas[14]) in both hits (**c**) and non-hits (**d**) (all $P > 0.05$). **e**, **f**, Mean non-huddling net modulation is uncorrelated with mating and self-grooming latency and total duration in hits (**e**) and non-hits (**f**) (all $P > 0.05$).

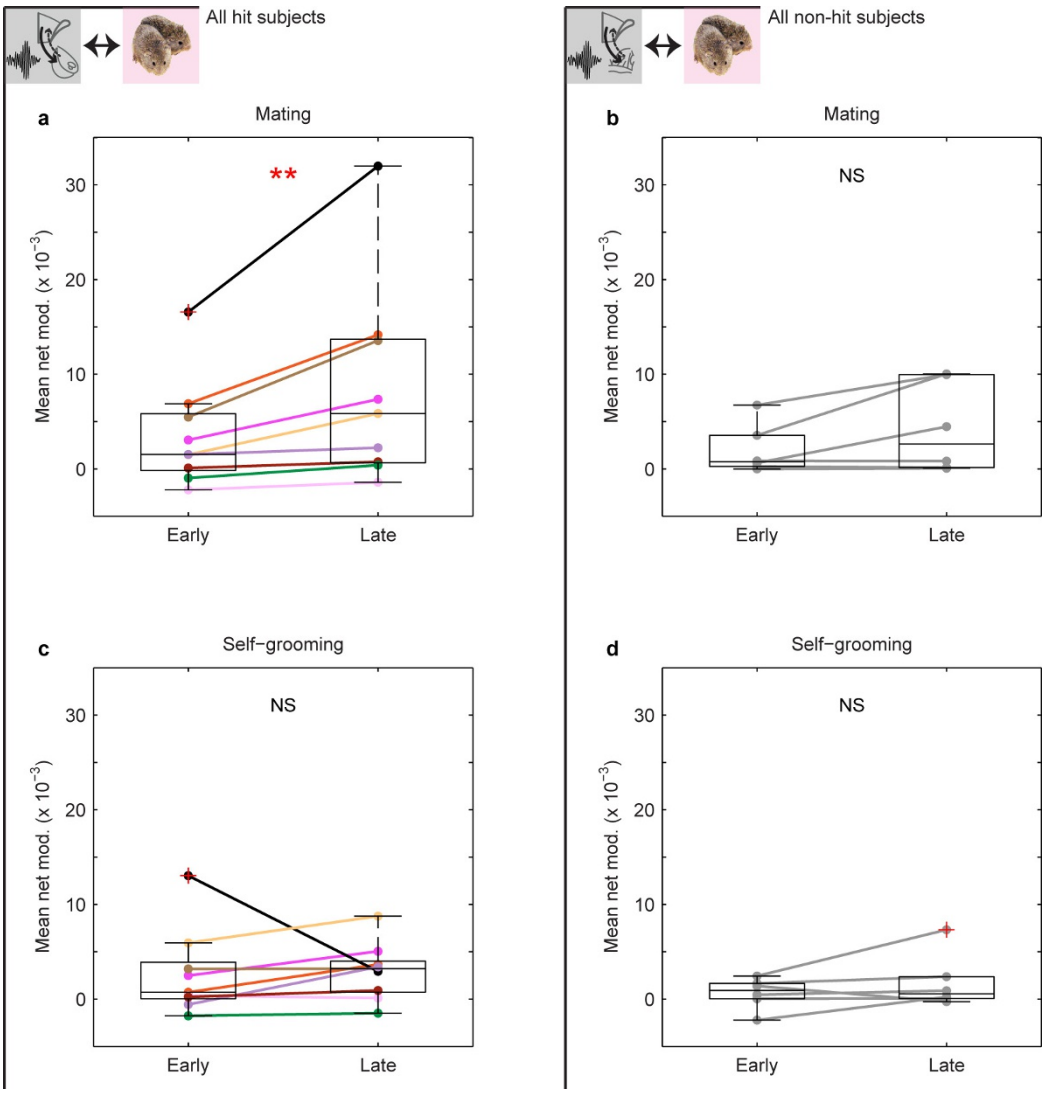

Extended Data Figure 7 | Net modulation during early and late mating and self-grooming. a, **b**, Mean net modulation during mating increases over time in hits (**a**; $n = 9$; $P = 0.008$) but not non-hits (**b**; $n = 6$; $P = 0.438$). **c**, **d**, Mean net modulation during self-grooming shows no significant change in either hits (**c**; $P = 0.406$) or non-hits (**d**; $P = 0.438$). P values in **a**–**d** are Bonferroni-corrected for multiple comparisons (see Methods). Mean early and late values for mating are derived from the first and last mating bouts. Mean values for self-grooming are derived from early and late self-grooming samples matched in number to the first and last mating bouts (see Methods). Boxplots show median and interquartile range.

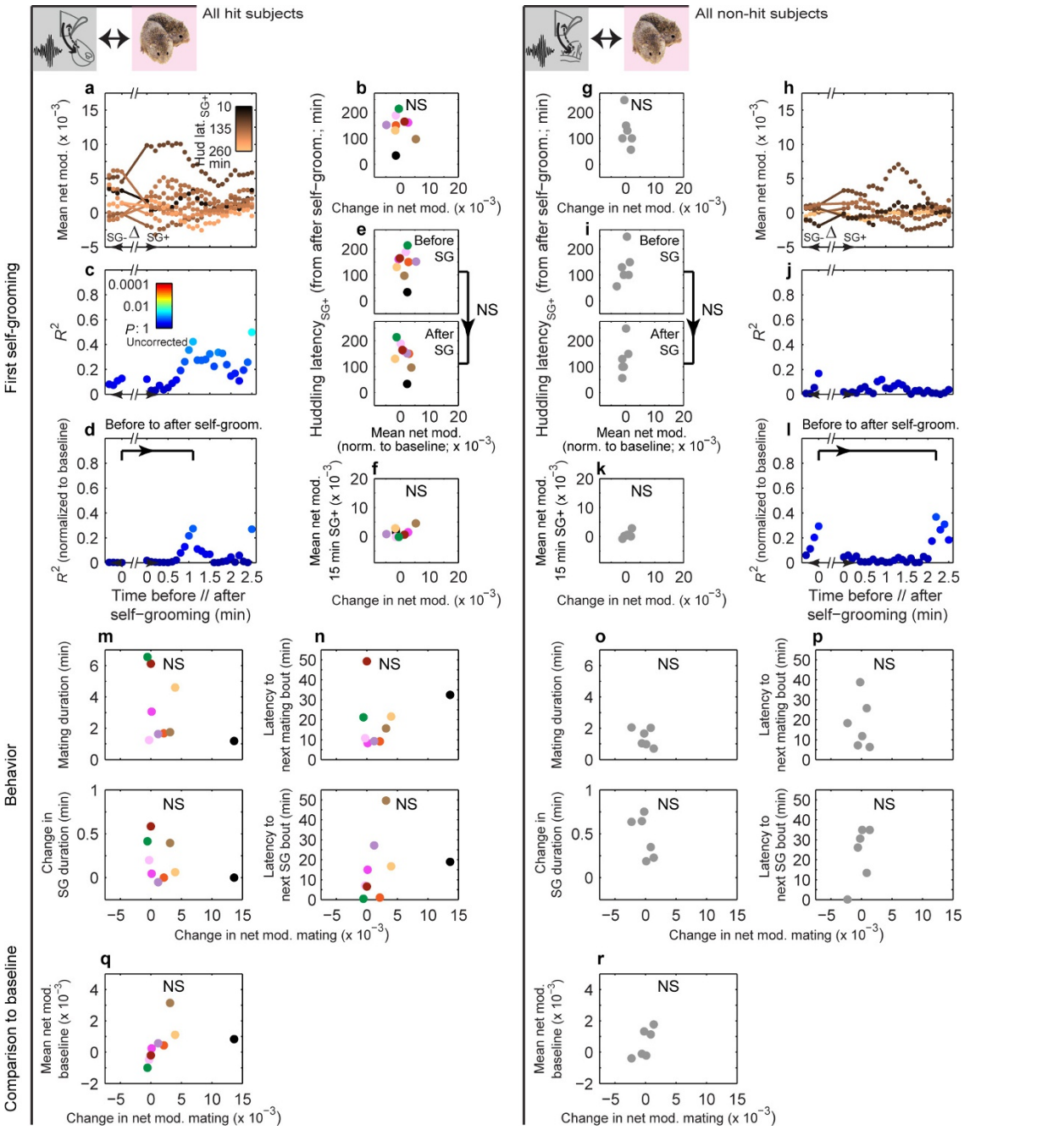

Extended Data Figure 8 | Behavioural specificity of correlation between local change in net modulation around mating and huddling latency. **a**, **h**, Mean non-huddling (NHud) net modulation values within 1 min moving windows (stepped by 0.1 min) before (SG−) and after (SG+) the first self-grooming bout of hits (**a**; $n = 9$) and non-hits (**h**; $n = 6$). Each subject's values are colour-coded by that subject's latency to huddle from the end of the self-grooming bout (latency$_{SG+}$). **b**, **g**, Change in mean net modulation from immediately before to after the first self-grooming bout is uncorrelated with huddling latency$_{SG+}$ in hits (**b**; $R^2 = 0.01$, $P = 0.787$; indicated by line segments in **a**) and non-hits (**g**; $R^2 = 0.27$, $P = 0.290$; line segments in **h**). **c**, **j**, Strength of correlation between mean net modulation and huddling latency$_{SG+}$ shows no consistent increase in either hits (**c**) or non-hits (**j**). **d**, **e**, **i**, **l**, Subtracting out the mean baseline net modulation from the local values around self-grooming confirms no significant increase in correlation strength in either hits (**d**, **e**; $P = 0.164$; permutation test on difference in R^2 (0.27) between bracketed time-points) or non-hits (**i**, **l**; $P = 0.655$, observed R^2 difference of 0.07). **f**, **k**, Change in mean net modulation from immediately before to after first self-grooming bout is uncorrelated with mean non-huddling net modulation in the 15 min after self-grooming in hits (**f**; $R^2 = 0.24$, $P = 0.180$) and non-hits (**k**; $R^2 = 0.55$, $P = 0.090$). **m**–**r**, Change in net modulation around first mating bout (Fig. 3e, j *x* axis) is uncorrelated with local behavioural parameters (change in self-grooming duration around bout and mating duration within bout) in hits (**m**) and non-hits (**o**) (all $P > 0.05$). It is further uncorrelated with the latency to next mating or self-grooming bouts (**n**, **p**) and the mean net modulation during the baseline solo period (**q**, **r**) in hits and non-hits (all $P > 0.05$).

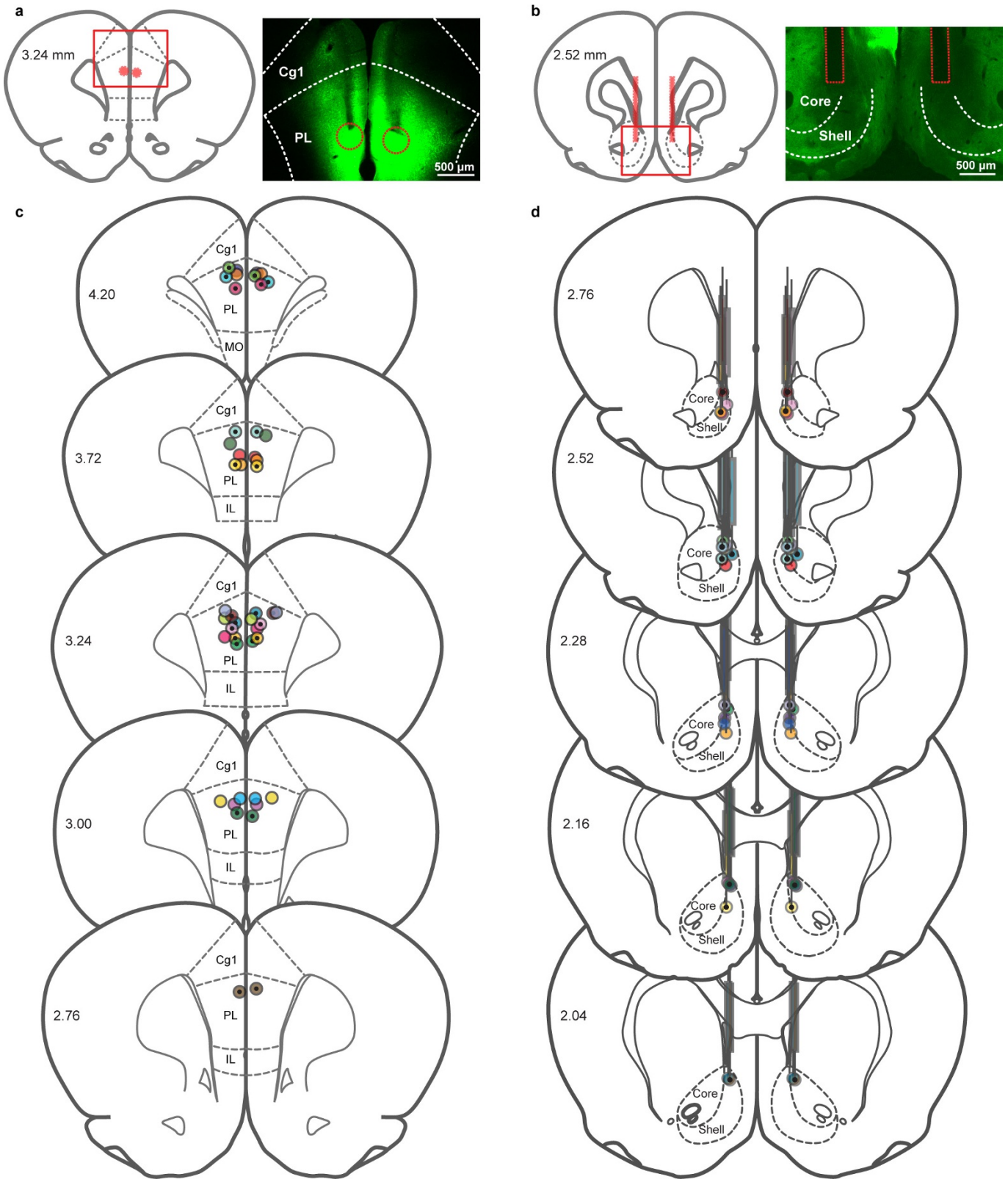

Extended Data Figure 9 | Validation of virus injection and optical implant locations. a, **b**, Representative coronal sections showing estimated centres of (**a**) bilateral virus injection and (**b**) optical implant placement for *in vivo* optogenetics subjects. Virus injection localization was based on minor tissue damage at dorsal-most surface of the coronal section where injection syringe initially entered the brain, the densest concentration of fluorescence, and physical tracts of damage left by injection syringe. Optical implant localization was based on physical tracts of damage left by optical implant. Morphology of corpus callosum was used to determine anterior/posterior position of injections and implants. **c**, Virus injection and (**d**) optical implant locations for all *in vivo* optogenetics subjects. ChR2-expressing subjects ($n = 12$) are indicated by circles with dotted centres. Control subjects ($n = 11$) are indicated by circles with empty centres. Each colour is a separate subject, with two circles per subject (bilateral injection and optical implant). All injection centre locations fell within the prelimbic cortex and all optical implant locations fell within the medial NAcc. In **a**–**d**, the anterior/posterior location of each section (units of rat brain atlas[14]) is indicated on left-hand side of the section. IL, infralimbic cortex; MO, medial orbital cortex.

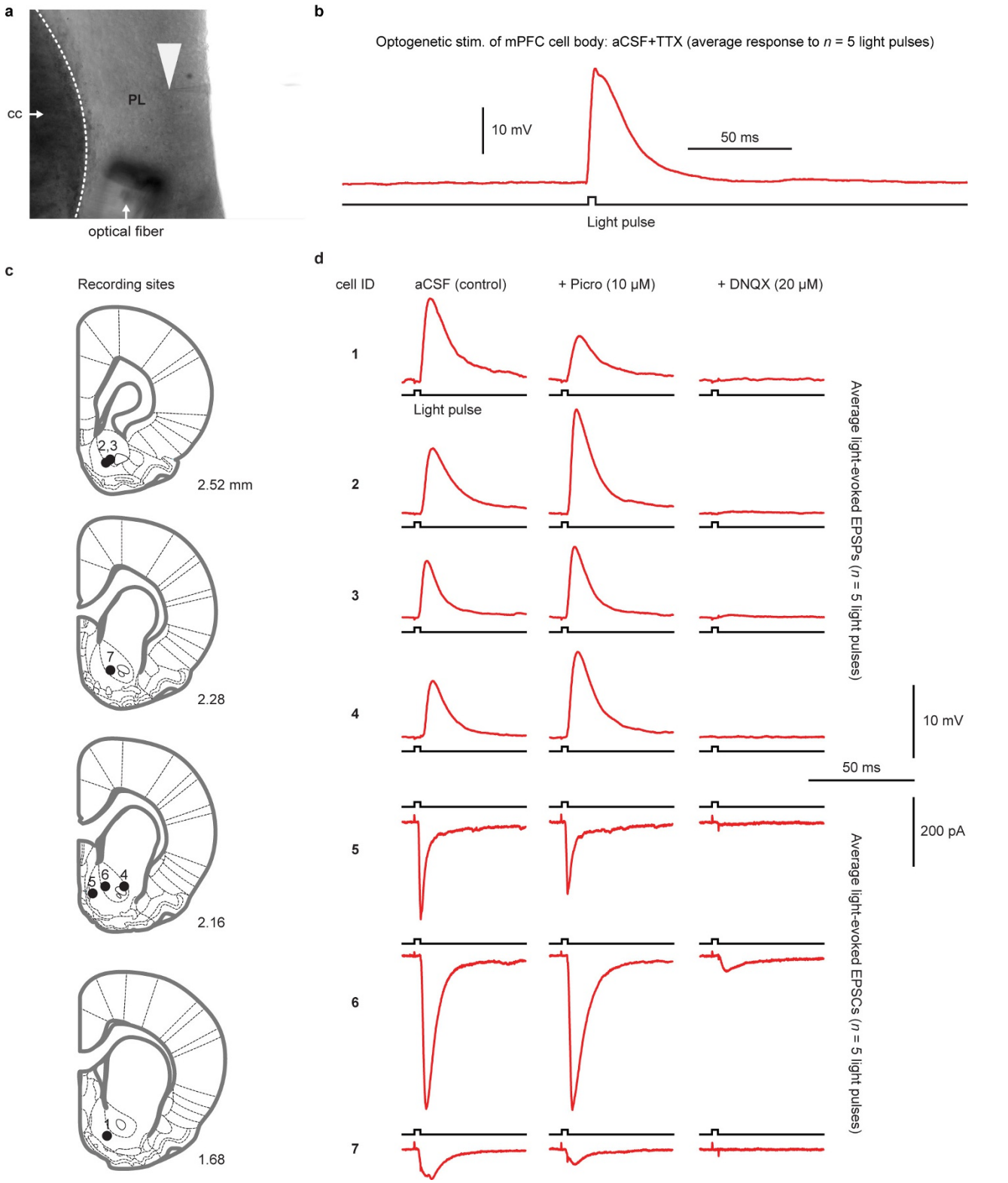

Extended Data Figure 10 | Validation of light-induced electrophysiological responses in mPFC and NAcc. a, Representative image of whole-cell patch-clamp recording from a prelimbic mPFC neuron cell body in slice preparation. Recording electrode (tip denoted with white arrowhead) is patched onto a cell, and an optical fibre is oriented towards the cell for optogenetic stimulation. **b**, Example light-evoked potential (average response to five, 1-ms light pulses; see Methods) in a prelimbic mPFC neuron in the presence of tetrodotoxin (TTX; 1 μM) to show a direct effect of light stimulation. **c**, Whole-cell patch-clamp recordings were obtained from $n = 7$ putative medium spiny neurons (from four subjects) in NAcc. Anterior/posterior location of each section (units of rat brain atlas[14]) indicated on bottom-right of the section. **d**, Average electrophysiological responses (excitatory postsynaptic potentials (EPSPs; cells 1–4) or currents (EPSCs; cells 5–7)) to five, 1-ms light pulses delivered onto the cell. Application of picrotoxin (Picro; second column) had no consistent effect on electrophysiological responses, whereas DNQX (third column) disrupted them, indicating that electrophysiological responses were due to glutamatergic transmission. Abbreviation 'cc', corpus callosum.